Published in final edited form as:

Mol Microbiol. 2017 March ; 103(6): 931–957. doi:10.1111/mmi.13613.

Suppression and Synthetic-Lethal Genetic Relationships of Δ*gpsB* Mutations Indicate That GpsB Mediates Protein Phosphorylation and Penicillin-Binding Protein Interactions in *Streptococcus pneumoniae* D39

Britta E. Rued[1,§], **Jiaqi J. Zheng**[1,§], **Andrea Mura**[2,3], **Ho-Ching T. Tsui**[1], **Michael J. Boersma**[1], **Jeffrey L. Mazny**[1], **Federico Corona**[2], **Amilcar J. Perez**[1], **Daniela Fadda**[2], **Linda Doubravová**[3], **Karolína Buriánková**[3], **Pavel Branny**[3], **Orietta Massidda**[2], and **Malcolm E. Winkler**[1,*]

[1]Department of Biology, Indiana University Bloomington, Bloomington, IN 47405, USA

[2]Dipartimento di Scienze Chirurgiche, Università di Cagliari, 09100 Cagliari, Italy

[3]Cell and Molecular Microbiology Division, Institute of Microbiology, v.v.i., Academy of Sciences of the Czech Republic, 142 20 Prague 4, Czech Republic

SUMMARY

GpsB regulatory protein and StkP protein kinase have been proposed as molecular switches that balance septal and peripheral (side-wall like) peptidoglycan (PG) synthesis in *Streptococcus pneumoniae* (pneumococcus); yet, mechanisms of this switching remain unknown. We report that Δ*divIVA* mutations are not epistatic to Δ*gpsB* division-protein mutations in progenitor D39 and related genetic backgrounds; nor is GpsB required for StkP localization or FDAA labeling at septal division rings. However, we confirm that reduction of GpsB amount leads to decreased protein phosphorylation by StkP and report that the essentiality of Δ*gpsB* mutations is suppressed by inactivation of PhpP protein phosphatase, which concomitantly restores protein phosphorylation levels. Δ*gpsB* mutations are also suppressed by other classes of mutations, including one that eliminates protein phosphorylation and may alter division. Moreover, Δ*gpsB* mutations are synthetically lethal with Δ*pbp1a*, but not Δ*pbp2a* or Δ*pbp1b* mutations, suggesting GpsB activation of PBP2a activity. Consistent with this result, co-IP experiments showed that GpsB complexes with EzrA, StkP, PBP2a, PBP2b, and MreC in pneumococcal cells. Furthermore, depletion of GpsB prevents PBP2x migration to septal centers. These results support a model in which GpsB negatively regulates peripheral PG synthesis by PBP2b and positively regulates septal ring closure through its interactions with StkP-PBP2x.

Graphical Abstract

[*]**Corresponding author:** Malcolm E. Winkler, Department of Biology, Indiana University Bloomington, 1001 E. 3rd St., Bloomington, IN 47405 USA, Phone: 812-856-1318, winklerm@indiana.edu.
[§]Contributed equally to this work.

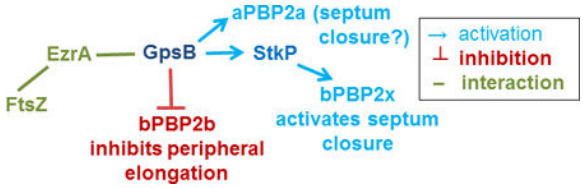

Model of GpsB protein interactions and coordination of septal and peripheral peptidoglycan synthesis in *Streptococcus pneumoniae*, indicating changes in the PhpP protein phosphatase that suppress the requirement for essential GpsB.

ABBREVIATED SUMMARY

GpsB is a small hexameric protein that is essential and acts to balance septal and sidewall-like peptidoglycan synthesis at the midcell of the ovoid-shaped bacterium *Streptococcus pneumoniae*, which is a serious human respiratory pathogen. Results from genetic, microscopic, physiological, and *in vivo* co-immunoprecipitation experiments reported herein support a model in which GpsB activates penicillin-binding proteins involved in septal ring closure and inhibits penicillin-binding proteins involved in elongation to maintain normal ovococcus cell shape and size.

Keywords

pneumococcal cell division; penicillin-binding protein (PBP) regulation; bacterial protein phosphorylation; bacterial protein phosphatases; DivIVA function

INTRODUCTION

GpsB has emerged as a major regulator of peptidoglycan (PG) biosynthesis in low-GC Gram-positive bacteria. GpsB contains a domain that is also found in DivIVA, which is a curvature-binding membrane protein that plays diverse roles in recruiting other proteins to the poles and division septa of rod-shaped bacteria (Claessen *et al.*, 2008, Kaval & Halbedel, 2012, Massidda *et al.*, 1998, Strahl & Hamoen, 2012, Tavares *et al.*, 2008). However, despite this shared region of homology, GpsB plays distinctly different roles from DivIVA in regulating PG biosynthesis in rod-shaped bacteria, including *Bacillus subtilis* (*Bsu*) and *Listeria monocytogenes* (*Lmo*) (see (Cleverley *et al.*, 2016, Rismondo *et al.*, 2016)). GpsB was initially characterized in *Bsu* by a screen for mutations that are synthetically lethal with deletion mutations that eliminate EzrA (Claessen *et al.*, 2008), which plays roles in modulating the dynamics of FtsZ-ring formation (see (Cleverley *et al.*, 2014, Land *et al.*, 2014)). In addition, Δ*gpsB* mutations are synthetically lethal with deletions that eliminate FtsA (Tavares *et al.*, 2008), which anchors the FtsZ ring to cell membranes and recruits downstream proteins required to complete the cell division process (see (Busiek & Margolin, 2015, Ortiz *et al.*, 2016)). Notably, mutations that eliminate GpsB, FtsA, or EzrA are singly not lethal in *Bsu*, although GpsB is required for growth in high-salt media (Claessen *et al.*, 2008, Tavares *et al.*, 2008).

Localization studies showed that GpsB assembles into the *Bsu* divisome at ≈ 20% of the cell cycle after FtsZ, FtsA, ZapA, and EzrA (Gamba *et al.*, 2009, Tavares *et al.*, 2008). In both

Bsu and *Lmo*, GpsB is a dynamic protein that cycles between the septum and side wall PG biosynthetic machines (Claessen *et al.*, 2008, Rismondo *et al.*, 2016). Bacterial two-hybrid (B2H) analyses indicated that *Bsu* GpsB potentially interacts with EzrA and with Class A penicillin-binding protein PBP1 (aPBP1), which catalyzes both transglycosylase (TG) and transpeptidase (TP) activities, as well as the side-wall regulator MreC (Claessen *et al.*, 2008). Consistent with these results, localization studies and characterization of Δ*gpsB* mutants showed that GpsB is required for normal localization and function of aPBP1 during the cell cycle and in pole maturation (Claessen *et al.*, 2008). Together, these findings led to the model that GpsB acts as a switching protein that shuttles aPBP1 away from poles to carry out PG elongation in the sidewall, whereas EzrA returns the GpsB-aPBP1 complex to division septa (Claessen *et al.*, 2008).

Recent studies have confirmed and further defined roles played by GpsB as a switch between modes of PG septal and elongation synthesis in rod-shaped Gram-positive species (Claessen *et al.*, 2008, Rismondo *et al.*, 2016). In *Lmo*, GpsB again was observed to dynamically locate between septal and peripheral PG synthesis sites (Rismondo *et al.*, 2016). Lack of *Lmo* GpsB allowed normal growth at 30°C, retarded growth at 37°C and caused cell elongation, and prevented growth altogether at 42°C (Rismondo *et al.*, 2016). *Lmo* GpsB is also required for full virulence in animal models of *Lmo* infection. Combination of Δ*gpsB* and Δ*divIVA* mutations resulted in a synergistic, severe cell morphology defect that was dissimilar to that of either single *Lmo* mutant. Significantly, a direct interaction between *Lmo* GpsB and aPBPA1, the homologue of *Bsu* aPBP1, was inferred from a synthetic-lethal genetic relationship between Δ*gpsB* and Δ*pbpA2*, which itself is synthetically lethal with Δ*pbpA1* (Rismondo *et al.*, 2016). Direct binding of a negatively charged groove in the structure of the amino-terminal domain of GpsB to the positively charged cytoplasmic amino-terminal domain of aPBP1(A1) was demonstrated by B2H and biochemical assays (Rismondo *et al.*, 2016). Together, these data support the hypothesis that GpsB acts as a switch protein to regulate aPBP1(A1) function and localization in rod-shaped bacteria (Claessen *et al.*, 2008, Rismondo *et al.*, 2016).

Structural studies show that GpsB is a cytoplasmic, membrane-associated hexamer that resembles a tripod structure (Cleverley *et al.*, 2016, Rismondo *et al.*, 2016). The amino terminal domains associate as a trimer of dimers, with each dimer containing amino acids required for domain dimerization, membrane binding, and binding to *Bsu* aPBP1 and *Lmo* aPBPA1 (Cleverley *et al.*, 2016, Rismondo *et al.*, 2016). The carboxyl-terminal domains associate as a dimer of homotrimeric, parallel coiled-coils. In *Bsu*, the carboxyl-terminal domains contain a threonine residue (T75) that is phosphorylated by the PrkC protein kinase, which does not seem to regulate *Bsu* cell division (Pompeo *et al.*, 2015), but rather plays a role in sporulation (Shah *et al.*, 2008). However, GpsB is required for PrkC kinase activity, and phosphorylation of GpsB may provide a negative feedback loop by reducing PrkC kinase activity (Pompeo *et al.*, 2015).

Streptococcus pneumoniae (*Spn*) GpsB also likely plays a role in switching between septal and peripheral PG synthesis, which emanate from the midcells of these ovoid cells (Massidda *et al.*, 2013, Land *et al.*, 2013, Fleurie *et al.*, 2014b). In primary, wild-type progenitor strains, such as virulent strains D39 and TIGR4 and isogenic unencapsulated

(Δ*cps*) derivatives of D39, GpsB is essential for growth (Land *et al.*, 2013). Depletion of GpsB in D39 Δ*cps* strains causes cultures to stop growing and eventually to lyse. GpsB-depleted cells elongate, enlarge, and contain multiple minimally constricted FtsZ and aPBP1a septal rings. These cell elongation and ring closure defects are consistent with a defect in controlling septal closure and cell elongation when GpsB is depleted (Land *et al.*, 2013). Another study of the requirement for *Spn* GpsB was performed in unencapsulated laboratory strain R6, which contains at least 81 mutations not found in the D39 progenitor background (Lanie *et al.*, 2007), and strain R800, which was derived from R6 (Fleurie *et al.*, 2014b). In contrast to recently derived D39 strains, GpsB was not essential in the R6 and R800 backgrounds, suggesting accumulation of suppressors in these laboratory strains that allow Δ*gpsB* mutants to grow.

In addition, *Spn* R800 Δ*gpsB* mutants showed several phenotypes that contrasted with phenotypes of *Bsu* or *Lmo* Δ*gpsB* mutants. In the *Spn* R800 strain, Δ*divIVA* mutations are epistatic to Δ*gpsB* mutations, in that the Δ*divIVA* Δ*gpsB* double mutant shows the same defective cell morphology as the Δ*divIVA* mutant compared to the Δ*gpsB* mutant (Fleurie *et al.*, 2014b). This observation was the basis for a model that GpsB acts as a negative regulator of DivIVA stimulation of cellular elongation, possibly through phosphorylation of DivIVA by the StkP kinase (Fleurie *et al.*, 2014b, Grangeasse, 2016). In contrast, this epistasis was not observed in *Lmo*, where Δ*gpsB*, Δ*divIVA*, and Δ*gpsB* Δ*divIVA* mutants show distinctively different defects in cell morphology (Rismondo *et al.*, 2016). In *Spn* R800 GpsB was reported to be required for localization of the StkP Ser/Thr protein kinase into division rings, whereas in *Bsu*, GpsB was not required for localization of the homologous PrkC protein kinase (Pompeo *et al.*, 2015). On the other hand, GpsB was required for optimal StkP and PrkC protein kinase activity in *Spn* and *Lmo*, respectively, suggesting that GpsB may positively regulate the activity of these protein kinases (Fleurie *et al.*, 2014b, Pompeo *et al.*, 2015). However, GpsB is phosphorylated by PrkC in *Bsu* (Pompeo *et al.*, 2015), whereas phosphorylation of GpsB by StkP has not been detected in *Spn* (Fleurie *et al.*, 2014b), and replacement of the putative phosphorylated threonine of *Lmo* GpsB with alanine did not produce a detectable phenotype (Cleverley *et al.*, 2016).

In this study, we tested several of the above hypotheses of GpsB function in an unencapsulated derivative of the D39 progenitor strain and in two other laboratory strains, R6 and Rx1, which were separately derived from the R36A unencapsulated mutant of strain D39 (see (Lanie *et al.*, 2007, Pozzi *et al.*, 1996)). With the exception of a requirement of GpsB for maximal protein phosphorylation, we found phenotypes of R800 Δ*gpsB* mutants could not be generalized to D39 and the other laboratory strains. In support of an involvement of GpsB in maximizing protein phosphorylation mediated by the StkP protein kinase, we report that lethal Δ*gpsB* mutations in the D39 progenitor strain are suppressed by mutations that inactivate the cognate PhpP protein phosphatase. This suppression analysis also revealed a new level of control that obviates the requirements for GpsB and for protein phosphorylation. We further show that GpsB activates aPBP2a activity and is required for migration of bPBP2x to the centers of division septa. Co-immunoprecipitation (co-IP) of complexes of proteins crosslinked in cells showed that GpsB resides in complexes with EzrA, StkP, aPBP2a, bPBP2b, and MreC and that StkP is in complexes with bPBP2x, as anticipated from a previous report (Morlot *et al.*, 2013). Together, our results suggest a

modified model of GpsB function as a mediator between septal closure and peripheral PG synthesis that accounts for the formation of large, elongated cells with unconstricted septal rings. In this model, GpsB activates StkP-bPBP2x and aPBP2a activities to close septal division rings and acts as a negative regulator of PG elongation by inhibition of bPBP2b and MreC activities.

RESULTS

divIVA mutations are not epistatic to *gpsB* mutations in pneumococcal strains R6 and D39

It was previously reported in laboratory strain R800 that Δ*divIVA* mutations are epistatic to Δ*gpsB* mutations (Fleurie *et al.*, 2014b). However, GpsB is not essential in unencapsulated laboratory strain R800 (Fleurie *et al.*, 2014b), whereas GpsB is essential in its wild-type, encapsulated, progenitor strain, D39 (Fleurie *et al.*, 2014b, Land *et al.*, 2013). These results suggest that domesticated laboratory strain R800 contains mutations that suppress primary phenotypes caused by Δ*gpsB* deletions and by mutations in other cell division genes (see (Land *et al.*, 2014, Land & Winkler, 2011, Tsui *et al.*, 2016)). As another example of these strain differences, changes of the single threonine residue in DivIVA (T201A) phosphorylated by StkP result in no morphology phenotype in D39 and two unencapsulated laboratory strains, R6 and Rx1, that were distantly derived from D39 (data not shown; Massidda *et al.*, 2013, Straume *et al.*, 2016), but cause cell elongation and polar bulges in R800 (Fleurie *et al.*, 2012). The normal frequency of transformation and colony morphology observed during construction of *divIVA*(T201A) mutants in D39 strains are not indicative of suppressor accumulation (data not shown).

Consequently, we tested whether the epistatic genetic relationship between *gpsB* and *divIVA* mutations reported in strain R800 is generalizable to progenitor strain D39 and other laboratory strains. We confirmed that laboratory strain R6 readily tolerates a Δ*gpsB* deletion, similar to R800 (Fleurie *et al.*, 2014b), whereas an Rx1 Δ*gpsB* mutant grows poorly (Table 1, lines 20 and 21). This result is consistent with accumulation of different combinations of mutations in different lines of laboratory strains derived from the D39 progenitor strain (Lanie *et al.*, 2007). In contrast, encapsulated strain D39 and isogenic unencapsulated D39 Δ*cps* derivatives do not grow when transformed with Δ*gpsB* mutations (Table 1, lines 1, 9, 13, and 17) (Fleurie *et al.*, 2014b, Land *et al.*, 2013). We next compared the cell morphologies of the R6 parent, the single R6 Δ*gpsB* or Δ*divIVA* mutant, and the R6 Δ*gpsB* Δ*divIVA* double mutant grown exponentially and stained with a fluorescent D-amino acid (FDAA) probe, which indicates regions in the peptidoglycan (PG) of active penicillin-binding protein (PBP) TP activity (Fig. 1A and 1B) (Boersma *et al.*, 2015, Kuru *et al.*, 2012, Kuru *et al.*, 2015). Because septal and peripheral (sidewall-like) PG synthesis are coordinated with FtsZ ring formation in *Spn*, FDAA-labeled bands serve as a surrogate for FtsZ ring assembly and localization (see (Boersma *et al.*, 2015, Tsui *et al.*, 2014)).

The R6 Δ*gpsB* mutant grew at the same rate, but formed larger, elongated cells, often with multiple FDAA-labeled rings, compared to the R6 parent (Fig. 1A and 1B, row 2). The vast majority (≥95%) of FDAA rings were parallel to each other and perpendicular to the long axis in R6 Δ*gpsB* cells, in contrast to R800 Δ*gpsB* cells, in which ≈ 25% of FDAA staining was reported in “Z-like” spiral patterns (Fleurie *et al.*, 2014b). The R6 Δ*divIVA* mutant

formed chains of large compacted, spherical cells containing parallel FDAA-labeled rings (Fig. 1B, row 3), as reported before (Fadda *et al.*, 2003, Fadda *et al.*, 2007). The R6 Δ*gpsB* Δ*divIVA* mutant grew considerably slower and formed large, elongated, misshapen cells with thick rings of FDAA labeling (Fig. 1A and 1B, row 4). We conclude that the Δ*gpsB* Δ*divIVA* mutant has a severe morphological defect distinct from those of either the Δ*gpsB* or Δ*divIVA* mutant and that the Δ*divIVA* mutation is not epistatic to the Δ*gpsB* mutation in laboratory strain R6. In addition, the Δ*gpsB* mutation did not cause severe FDAA ring mislocalization in the R6 strain, as reported in the R800 strain (Fleurie *et al.*, 2014b).

These conclusions were confirmed by similar experiments in the D39 progenitor genetic background and in the Rx1 laboratory strain, which exhibits a mutator phenotype (Table S1). D39 Δ*gpsB* and Rx1 Δ*gpsB* mutants do not grow or grow poorly (Table 1, lines 1, 9, 13, 17, and 21), respectively, and acquire suppressor (*sup*) mutations, which are described and characterized below (Table 2). In either background, the Δ*gpsB* (*sup*) mutants grew similarly to the parent strains and formed cells containing parallel FDAA-labeled rings (below; Fig. 1C and 1B, rows 5 and 6; Fig. S1, rows 1 and 2). The Rx1 Δ*gpsB sup4* mutant formed longer cells with multiple division rings compared to the Rx1 parent strain (Fig. S1, rows 1 and 2), and >95% of Rx1 Δ*gpsB sup4* cells expressing FtsZ-mCherry from a single chromosomal locus had parallel FtsZ rings perpendicular to their long axis (data not shown), similar to the pattern of FDAA labeling (Fig. S1, row 2). In both the D39 Δ*cps* and Rx1 backgrounds, Δ*divIVA* mutants showed the expected phenotype of chains of enlarged, rounded cells (Fig. 1B, row 7 and Fig. S1, row 3). Again, Δ*gpsB* (*sup*) Δ*divIVA* double mutants of the D39 Δ*cps* and Rx1 strains showed the distinct, severe defects in cell morphology described above for the R6 strain (Fig. 1B, rows 4 and 8; Fig. S1B row 4). Similar to the R6 double mutant, D39 Δ*cps* double mutants had reduced growth rates (Fig. 1C, rows 6–8). Interestingly, the Rx1 double mutant did not have a reduced growth rate compared to the Rx1 single mutants, but was delayed in stationary lysis (Supporting Information Fig S1A, rows 2–4). We conclude that an epistatic genetic relationship between *gpsB* and *divIVA* mutations does not exist in the D39 progenitor strain or in laboratory strains, other than R800, and that there is no genetic evidence that GpsB acts as a negative regulator of DivIVA stimulation of cellular elongation (Fleurie *et al.*, 2014b).

Δ*gpsB* mutations are suppressed by *phpP* Ser/Thr phosphatase mutations in strain D39

Transformation of a D39 Δ*cps* strain with a Δ*gpsB* amplicon infrequently led to the appearance of faster growing suppressor mutants (Table 2, lines 1–3 and 5). We sequenced the genomes of three independently isolated, spontaneous D39 Δ*cps* Δ*gpsB* suppressor mutants, which had similar growth rates as the parent strain in BHI broth (Table 2, lines 1–3). One of the suppressor mutants contained a single amino acid change (G229D) in *phpP*, which encodes the only canonical PP2C Ser/Thr phosphatase encoded by *Spn* (Table 2, line 1; Fig S2A) (Beilharz *et al.*, 2012, Novakova *et al.*, 2005, Osaki *et al.*, 2009). The other two *sup2* and *sup3* suppressor strains had intact copies of the $stkP^+$ and $phpP^+$ genes, but contained large deletions and adjacent duplications in the *spd_1034* region of the chromosome (Fig. S3). Additional independent Δ*gpsB* suppressors were isolated containing mutations in *phpP*, including *phpP*(L148S) in strain Rx1, or deletions in the *spd_1034* region of the chromosome, as well as other classes of Δ*gpsB* suppressor strains that lack the

latter mutations (Table 2, lines 4 and 5). This paper focuses primarily on the *phpP*(G229D) and related suppressor mutations.

The previous characterization of R800 Δ*gpsB* mutants reported that protein phosphorylation was eliminated in the absence of GpsB (Fleurie *et al.*, 2014b). The isolation of the *phpP*(G229D) and other putative suppressor mutations in *phpP* (Table 2, lines 1 and 4) led to the hypothesis that growth of the D39 Δ*cps* Δ*gpsB* mutant was accompanied by a decrease in protein de-phosphorylation that restored protein phosphorylation levels in the Δ*gpsB* mutant. Given the major phenotypic differences described above for laboratory strain R800, we first determined the effects of GpsB absence or depletion in the R6 and Rx1 or D39 backgrounds, respectively (Fig. 2). A Δ*gpsB* mutation reduced phosphorylation of DivIVA or StkP/MapZ(LocZ), which were not resolved on these gels, by ≈3–5× or ≈2–5×, respectively, compared to background levels in the Rx1 and R6 strains (Fig. 2A, lanes 3 and 5; Table S5). Likewise, depletion of GpsB in strain D39 caused ≈ 3–5× reduction in protein phosphorylation (Fig. 2B, lanes 1–2 versus 7–9; Table S6). Consistent with the above hypothesis, protein phosphorylation levels were restored to slightly above the wild-type level in the suppressed D39 Δ*gpsB sup1* (*phpP*(G229D)) mutant (Fig. 3, lane 4; Table S7). Likewise, protein phosphorylation was restored in the fast-growing Rx1 Δ*gpsB sup4* suppressed strain (Fig. 2A, lane 2; Table S5), containing the spontaneous *phpP*(L148S) mutation (Table 2, line 4; Fig. S2A). Moreover, purified PhpP(G229D) and PhpP(L148S) lacked protein phosphatase activity in biochemical assays (Fig. S4), but were properly folded compared to wild-type PhpP based on circular dichroism (CD) spectra and thermal denaturation analyses (data not shown). Unexpectedly, the D39 Δ*gpsB sup2* and *sup3* deletion mutants (Table 2) completely lacked protein phosphorylation (Fig. 3, lanes 2 and 3), despite encoding an intact *phpP*$^{+}$-*stkP*$^{+}$ operon.

To confirm that the *phpP*(G229D) mutation is solely responsible for Δ*gpsB* suppression in the *sup1* strain, we reconstructed the suppressed strain by two different genetic schemes (Fig. 4). Conserved G229 points toward R13 and the Mn^{2+} binding pocket in the predicted active site of PhpP (Rantanen *et al.*, 2007), and purified PhpP(G229D) lacks protein phosphatase activity (Fig. S4). In these schemes, we included another *phpP*(D192A) allele that inactivates PhpP function by interfering with Mn^{2+} binding in the active site (Fig. S4 and S5) (Novakova *et al.*, 2005, Rantanen *et al.*, 2007). In the first scheme (Fig. 4A), allele exchange (Sung *et al.*, 2001) was used to replace a *kan-rpsL*$^{+}$ Janus cassette inserted between *phpP*$^{+}$ and *stkP*$^{+}$ (Fig. S2B) with the *phpP*(G229D) or *phpP*(D192A) mutation in an unencapsulated derivative of strain D39. Notably, *phpP*(G229D) *stkP*$^{+}$ and *phpP*(D192A) *stkP*$^{+}$ mutants corresponded to tiny-colony transformants, whereas *phpP*$^{+}$ *stkP*$^{+}$ recombinants or a spontaneous *phpP*(G229D) *stkP*(G10stop) mutant formed normal- or medium-size colonies, respectively (Fig. 4A and Table 1, lines 10–12). Transformation of the slow-growing *phpP*(G229D) *stkP*$^{+}$ and *phpP*(D192A) *stkP*$^{+}$ mutants with a Δ*gpsB* amplicon was tolerated and resulted in faster growing colonies than the *phpP* mutant strains (Fig. 4A; Table 1, lines 11–12). Similar slow growth and restoration by a Δ*gpsB* mutation were observed for encapsulated D39 *phpP*(G229D) *stkP*$^{+}$ and *phpP*(D192A) *stkP*$^{+}$ mutants (Table 1, lines 18–19). Finally, the Δ*gpsB* mutation restored growth to a Δ*phpP*::P_c-*erm* mutant (Table 1, lines 4 and 14). The Δ*phpP*::P_c-*erm* mutation was polar and considerably reduced the amount of StkP (≈ 10×) (Fig. S7B, last lane), possibly by uncoupling translation

between *phpP* and downstream *stkP* (Fig. S2A). The decreased amount of StkP without PhpP lowered the amount of phosphorylated StkP/LocZ detected, whereas a wild-type level of phosphorylated DivIVA was maintained in *gpsB*$^+$ and Δ*gpsB* strains (Fig. 3, lane 7; data not shown), likely because of repeated catalytic rounds of DivIVA phosphorylation by StkP.

Since non-polar *phpP*(G229D) *stkP*$^+$ and *phpP*(D192A) *stkP*$^+$ mutants exhibit a severe growth defect, there is the possibility of selecting for additional suppressor mutations before growth is stabilized by transformation with a Δ*gpsB* mutation. We suspect that the normal growth reported previously for non-polar D39 Δ*phpP* mutants (Agarwal *et al.*, 2012) was due to suppressor accumulation, because D39 Δ*cps phpP*(G229D) *stkP*$^+$ or *phpP*(D192A) *stkP*$^+$ mutants exhibited improved growth upon repeated culturing (data not shown). To avoid suppressor accumulation, we devised a second genetic scheme to test suppression of a Δ*gpsB* mutation by the *phpP*(G229D) or *phpP*(D192A) mutations (Fig. 4B). In this scheme, a Δ*gpsB* // P_{fcsK}-*gpsB*$^+$ merodiploid was depleted for GpsB expression by removing the inducer fucose at the same time as transformation with a *phpP*(G229D) or *phpP*(D192A) amplicon. Transformants, which were maintained without fucose to deplete GpsB, each contained only the *phpP*(G229D) or *phpP*(D192A) mutation, but not the *phpP*$^+$ recombinant, and remained *stkP*$^+$ (Fig. 4B). The resulting strains, which were minimally stressed during construction, were converted to Δ*gpsB* by removing the ectopic copy of P_{fcsK}-*gpsB*$^+$. The reconstructed Δ*gpsB phpP*(G229D) mutant grew similarly to its parent and the original Δ*gpsB sup1* mutant (Fig. 5A). We observed that the lengths and widths of these Δ*gpsB phpP*(G229D) mutant cells were shorter than those of the wild-type parent strains, resulting in small cells with similar aspect ratios as the wild-type parent strains (Fig. 5B and 5C). Western blotting showed that cells of reconstructed Δ*gpsB phpP*(G229D) and Δ*gpsB phpP*(D192A) mutants contained approximately the same amounts of PhpP and StkP protein as their isogenic parent strains (Fig. S6). Finally, the reconstructed Δ*gpsB phpP*(G229D) mutant showed a similar restoration of protein phosphorylation as the original Δ*gpsB sup1* (*phpP*(G229D)) mutant (Fig. 3, lanes 1, 4–6). We conclude that single-amino acid changes that inactivate PhpP protein phosphatase can restore the growth of Δ*gpsB* mutants, probably by restoring protein phosphorylation decreased by the absence of GpsB.

Δ*gpsB* mutations are suppressed by additional classes of mutations

One class of Δ*gpsB* suppressors (*sup2* and *sup3*, Table 2, lines 2 and 3) contained wild-type *phpP*$^+$ and *stkP*$^+$ genes and large deletion-insertions in the *spd_1034* region of the chromosome (Fig. S3); yet, these strains lacked detectable protein phosphorylation (Fig. 3, lanes 2–3), despite expressing nearly wild-type levels of the StkP and PhpP proteins (data not shown). None of the genes in the two large deletions had obvious functions in protein phosphorylation or de-phosphorylation (Fig. S3, Table S8). A constructed Δ[*spd_1029–spd_1037*] deletion, similar to the one in the Δ*gpsB sup3* suppressed strain (Table 2, line 3; Fig. S3), did not alter protein phosphorylation levels compared to the parent strain or restore growth to a Δ*gpsB* mutant (Fig. S8; data not shown). The large chromosomal duplications adjacent to the deletions (Fig. S3) encode one reading frame annotated as a putative phosphoserine phosphatase (SPD_RS05380) (Table S8). However, overexpression of SPD_RS05380 by itself from a zinc-inducible promoter (strain IU12059, Table S1) did not lead to a detectable change in protein phosphorylation levels or suppress Δ*gpsB* in the D39

background (data not shown). We conclude that some combination of gene expression changes in these complicated insertion-duplication mutants likely caused the unanticipated lack of protein phosphorylation and compensated for the lack of GpsB in the *sup2* and *sup3* suppressor strains.

The lack of protein phosphorylation in the Δ*gpsB sup2* and Δ*gpsB sup3* mutants prompted us to test whether the growth defect of Δ*gpsB* mutants could be suppressed by the absence of protein phosphorylation in *stkP* mutants. We could transform Δ*gpsB* amplicons into Δ*stkP*, Δ*phpP-stkP*, and *phpP*(G229D) *stkP*(G10stop) mutants in the unencapsulated and encapsulated D39 genetic background (Table 1, lines 5–8, 10, and 15–16). The variable range of transformant recovery in the Δ*phpP*, Δ*stkP*, and Δ*phpP-stkP* mutants (Table 1) was consistent with a previous report (Echenique *et al.*, 2004), and Western-blot controls confirmed the lack of the StkP and PhpP proteins and protein phosphorylation in these mutants (Fig. 2, 3, and S7). However, interpretation of these results was problematic, because the Δ*stkP*, Δ*phpP-stkP*, and *phpP*(G229D) *stkP*(G10stop) mutants in strain D39 are genetically unstable (see (Massidda *et al.*, 2013)). Upon restreaking and regrowth, these mutants show heterogeneous colony sizes and faster growth properties, indicative of suppressor accumulation (data not shown). Therefore, it is likely that the D39 Δ*stkP* mutants accumulated additional suppressor mutations that bypassed the requirement for GpsB. In this study, we did not identify these putative suppressors or how they could suppress the requirement for GpsB.

GpsB and StkP have different, but overlapping localization patterns at each division stage, and GpsB is not required for StkP localization in septal rings

To understand the relationship between GpsB and StkP detected in the genetic experiments described above, we performed 2D IFM to localize GpsB-FLAG or GpsB-L-FLAG^3 relative to StkP and StkP-HA in the same cells (Fig. 6) Previously we used 2D IFM to localize GpsB-FLAG relative to FtsZ-Myc in pneumococcal D39 cells at different stages of division (Land *et al.*, 2013). The strain expressing GpsB-FLAG exhibited growth (35 min doubling time; equal growth yield) and cell morphology comparable to the parent strain (Fig. 6A and 6B), in contrast to a GFP-GpsB fusion reported in the R800 background (Fleurie *et al.*, 2014b). A further indication that *Spn* GpsB-FLAG is nearly fully functional is that amino acid changes in the C-terminal domain of GpsB cause loss of GpsB function (unpublished result; Cleverley *et al*, 2016). The GpsB-L-FLAG^3-expressing strain grew like the parent strain, but formed cells that were slightly longer (1.1×) than those of the parent (Fig. 6A and 6C). As reported previously (Land *et al.*, 2013), GpsB localization is somewhat diffuse at early division stages, localizes over the hemispheres of newly divided cells, persists at division septa, and is diffuse around the equators of new daughter cells (Fig. 6B, 6C, 6E, and 6F). This localization pattern overlaps, but is different from that of FtsZ, which exhibits distinct rings in early-division cells, and leaves septa before PBPs and other proteins for the equators of the daughter cells (Land *et al.*, 2013, Tsui *et al.*, 2014), presumably directed by MapZ(LocZ) (Fleurie *et al.*, 2014a, Holečková *et al.*, 2015). Consistent with a previous report (Tsui *et al.*, 2014), StkP localizes differently from either FtsZ or GpsB, and remains at closing septa with PBPs after FtsZ and GpsB have started to move to the equators of the

daughter cells (Fig. 6A–6E). We conclude that GpsB and StkP have different localization patterns that overlap at each stage of the cell cycle.

Consistent with this partial difference in localization, we did not find that GpsB is required for StkP localization to division rings in the R6 and Rx1 laboratory strains and in the progenitor D39 genetic background (Fig. 7 and S9). In the R800 laboratory strain, the absence of GpsB led to diffuse, mislocalization of StkP to cell peripheries instead of to division rings (Fleurie *et al.*, 2014b). In contrast, StkP-FLAG[2] localized to rings in a large majority of R6 Δ*gpsB* cells (Fig. 7, lines 1–2) and in D39 Δ*cps* cells depleted for GpsB (Fig. 7, lines 3–4). Similarly, GFP-StkP localized in defined bands in the majority of Rx1 Δ*gpsB* cells containing the *phpP*(L148S) suppressor mutation (Fig. S9B). Thus, StkP still localizes in the majority of cells to rings perpendicular to the long axis of elongated, sometimes irregularly shaped cells lacking or depleted for GpsB. On the other hand, we did notice that GpsB-L-FLAG[3], but not GpsB-FLAG, causes some mislocalization of StkP-HA that was not observed when StkP was detected directly with anti-StkP antibody (Fig. 6F compared to Fig. 6B–6E). Moreover, StkP occasionally was detected in aberrant patches away from division rings in elongated cells lacking or depleted for GpsB (Fig. 7, rows 2 and 4; Fig. S9B). Taken together, these results indicate that GpsB is not necessary for StkP ring formation, but GpsB and StkP are likely in a complex together during at least one stage of cell division. This conclusion was supported by *in vivo* co-IP experiments presented below.

Δ*gpsB* and Δ*pbp1a* mutations are synthetically lethal in *Spn*

Besides possible interactions between GpsB and StkP, recent genetic and biochemical experiments demonstrate that GpsB controls and is required for aPBPA1, but not aPBPA2, activity in *Lmo* (*Introduction*) (Cleverley *et al.*, 2016, Rismondo *et al.*, 2016). Similar to *Lmo*, either *Spn* aPBP1a or aPBP2a is required for growth, and they cannot be inactivated at the same time (Hoskins *et al.*, 1999, Paik *et al.*, 1999). However, aPBP1a and aPBP2a are not functionally equivalent as illustrated by the markedly smaller cells formed by Δ*pbp1a* compared to Δ*pbp2a* mutants (Land & Winkler, 2011, Tsui *et al.*, 2016). Based on the precedent from *Lmo*, we tested for a synthetic lethal relationship between GpsB and the three aPBPs of *Spn* (Table 3). In the R6, Rx1, and the suppressed D39 Δ*gpsB phpP*(G229D) strains, there is a clear synthetic lethal genetic relationship between Δ*gpsB* and Δ*pbp1a* mutations, but not Δ*pbp2a* or Δ*pbp1b* mutations (Table 3). Thus, either aPBP1a or aPBP2a is required for viability. Likewise, either aPBP1a or GpsB is required for viability, implying that GpsB is required for aPBP2a activity, since GpsB is not a PBP.

GpsB depletion prevents migration of bPBP2x TP activity to the centers of division septa

Depletion of GpsB in D39-derived strains results in elongated cells containing rings of FtsZ and aPBP1a that fail to contract (Land *et al.*, 2013). Previous surface plasmon resonance (SPR) experiments suggest a potential interaction between GpsB and StkP (Fleurie *et al.*, 2014b). Moreover, StkP binds Class B PBP2x (bPBP2x) (Morlot *et al.*, 2013), which carries out septal ring closure (Giefing *et al.*, 2010, Land *et al.*, 2013, Morlot *et al.*, 2013, Peters *et al.*, 2014, Tsui *et al.*, 2014), although bPBP2x is not known to be phosphorylated by StkP (Morlot *et al.*, 2013). The interactions among GpsB, StkP, and bPBP2x suggests that the defect in ring closure when GpsB is depleted could be caused, in part, by an inability of

bPBP2x to move to the centers of division septa during cell division (Tsui *et al.*, 2014). To test this hypothesis, we labeled wild-type and Δ*gpsB*//P_{fcsK}-*gpsB*$^{+}$ merodiploid cells with an FDAA and then examined localization of bPBP2x TP activity, which we showed migrates to the centers of septa of mid-to-late divisional cells, separately from other PBP TP activities (Fig. 8) (Tsui *et al.*, 2014). Consistent with previous results, bPBP2x TP activity accumulates as a dot of FDAA labeling at the centers of septa of wild-type cells and the merodiploid expressing GpsB protein in the presence of the inducer, fucose (arrows, Fig. 8A and 8B). In contrast, merodiploid cells depleted for GpsB (no fucose, Fig. 8C) elongate, contain rings of FDAA labeling that fail to contract, and lack detectable migration of bPBP2x TP activity to the centers of septa. We conclude that GpsB is required for division ring closure and migration of bPBP2x TP activity to the centers of septa.

GpsB is in complexes with EzrA, StkP, aPBP2a, bPBP2b, and MreC during stages of cell division

Previous B2H assays indicated putative interactions between pneumococcal GpsB and EzrA or DivIVA, but not with FtsZ (Fleurie *et al.*, 2014b). Pairwise binding assays of purified proteins using SPR indicated possible interactions between pneumococcal GpsB and DivIVA (Fleurie *et al.*, 2014b). B2H assays have suggested interactions between *Bsu* GpsB and EzrA, PrkC (protein kinase), PBP1, or MreC (Claessen *et al.*, 2008, Pompeo *et al.*, 2015). A putative interaction between *Bsu* GpsB and DivIVA was detected in one study (Pompeo *et al.*, 2015), but not another (Claessen *et al.*, 2008). SPR and B2H assays have defined the interaction between *Bsu* and *Lmo* GpsB and the positively charged amino-terminus of aPBP1 and aPBPA1, respectively (Claessen *et al.*, 2008, Rismondo *et al.*, 2016). To date, probing of *in vivo* complexes containing GpsB have not been reported for any bacterium.

To gain information about *in vivo* complexes containing pneumococcal GpsB and StkP, we crosslinked exponentially growing cells with formaldehyde and performed pull-down experiments on anti-FLAG magnetic beads of epitope-tagged, bait proteins, GpsB-L-FLAG^{3}, StkP-FLAG^{2}, or EzrA-L-FLAG^{3}, expressed from their normal chromosomal loci (Table 4; *Experimental procedures*). Control experiments showed that ≈ 55% of the GpsB-L-FLAG^{3} protein in cell lysates was retained by the beads (data not shown). Following elution from beads, crosslinks were broken by heating, and proteins in complexes were detected pairwise by Western blotting using native antibodies to StkP, MreC, FtsA, FtsZ, or PhpP or to HA or Myc epitope tags attached to prey proteins (Table 4). Strains containing two epitope-tagged proteins exhibited minimal cell morphology or growth defects (Fig. 6E and 6F). Control mock pull downs were run on crosslinked cells that did not express the GpsB-L-FLAG^{3} bait protein and were used as a background control. Additional control experiments demonstrated that intact PG rings labeled with FDAA and Z rings of FtsZ-GFP were maintained in cells during the crosslinking procedure (data not shown).

In a typical experiment (Fig. 9A and S10), Western blots were run on the starting cell lysates before loading onto the beads (Fig. S10A) and on the eluted prey proteins that were in crosslinked complexes with the bait protein (Fig. 9A). Complexes containing GpsB together with bPBP2b, StkP, and/or aPBP2a, but not bPBP2x, were detected in this example. A

control Western blot showed that nearly all of the bPBP2x-HA that was loaded onto beads from the cell lysate was recovered in the loading supernates ("flow-through") fraction, ruling out degradation (data not shown). Recovery of prey proteins was quantitated relative to background areas in the mock control lanes from cells not expressing bait proteins (Table 4), where a 2-fold ratio was the limit of detection for this method. Co-IP experiments with StkP-FLAG[2] as bait were also performed and quantitated (Table 4). A complex containing EzrA and FtsZ was also confirmed as part of a study of EzrA function and interactions that will be presented elsewhere (Amilcar Perez, in preparation). Finally, we repeated B2H assays to confirm likely direct interactions between GpsB and EzrA (Table 4; Fig. S15). The *in vivo* interaction map from these experiments of pneumococcal GpsB and StkP is summarized in Figure 9B and discussed below.

DISCUSSION

Roles of GpsB in modulating septal and peripheral PG synthesis in *Spn*

Results presented in this paper support a central role for GpsB in mediating a balance between septal and peripheral PG biosynthesis in *Spn* cell division. Determinations of protein phosphorylation levels and new suppressor analyses (Fig. 2–4; Table 2) support the previous conclusion that GpsB is required for maximal protein phosphorylation in exponentially growing cells (Fleurie *et al.*, 2014b, Grangeasse, 2016). GpsB is also required for optimal protein phosphorylation in *Bsu* (Pompeo *et al.*, 2015), suggesting that GpsB regulates protein phosphorylation levels in several Gram-positive species. In addition, synthetic-lethality relationships (Table 3), protein localization (Fig. 6 and 8), and *in vivo* crosslinking-coIP experiments (Fig. 9) show that pneumococcal GpsB activates aPBP2a, is required for septal ring closure by bPBP2x, and is present in complexes with aPBP2a and bPBP2b at stages of the division cycle. These results support and extend previous models based on *Bsu* and *Lmo* GpsB that GpsB directly interacts and regulates PBP activities (Claessen *et al.*, 2008, Cleverley *et al.*, 2016, Rismondo *et al.*, 2016).

Combined results from *in vivo* co-IP experiments indicate that GpsB acts as a central signaling complex poised between the EzrA in the divisome and the PBPs in the septal and peripheral PG machines, as first proposed in *Bsu* (Claessen *et al.*, 2008) and extended to *Spn* (Fleurie *et al.*, 2014b). As will be published elsewhere, *Spn* EzrA is in complexes *in vivo* with GpsB, FtsZ, FtsA, and other divisome proteins, including DivIVA (Amilcar Perez, in preparation). In contrast, complexes containing EzrA and PBPs have not yet been detected by *in vivo* co-IP, whereas complexes containing GpsB and three PBPs were readily detected (see below; Fig. 9 and 10). Complex detection reflects relative amounts of proteins and whether interactions are direct or indirect, strong or weak, and frequent or infrequent at different division stages. The interaction map emerging from these studies is consistent with a model in which interactions between EzrA and GpsB play a primary role in linking the dynamics of the divisome to PBP regulation.

Epistasis analyses presented here (Figs 1 and S1) do not support a general role for GpsB as a negative regulator of DivIVA activity in peripheral PG synthesis in progenitor *Spn* strain D39 or laboratory strains except for R800 (Fleurie *et al.*, 2014b). Putative interactions between *Spn* GpsB and DivIVA are detected by B2H analysis expressed in *E. coli* (Fig. S15)

(Fleurie *et al.*, 2014b), but detection of GpsB in a complex with DivIVA was below the limit of detection of the *in vivo* co-IP approach used here (Table 4; Fig. S12). The shorter and rounder appearance of *Spn* Δ*divIVA* mutant cells in chains (Fig. 1) suggests a defect in peripheral or in polar PG biosynthesis, as proposed in several papers (Boersma *et al.*, 2015, Fadda *et al.*, 2007, Fleurie *et al.*, 2014b, Massidda *et al.*, 2013, Straume *et al.*, 2016), but the exact function of DivIVA in *Spn* remains to be determined.

Effects of genetic backgrounds on *gpsB* mutant phenotypes

The differences in GpsB phenotypes in D39 and laboratory strains undoubtedly reflect the accumulation of bypass suppressors in the domesticated laboratory strains, which have been optimized to study processes, such as competence. Initial sequencing showed that different isolates of encapsulated, virulent D39 strains stored apart for decades have essentially the same genome sequences (Lanie *et al.*, 2007). Encapsulated D39 was the progenitor of unencapsulated mutant R36A, from which laboratory strains R6 and Rx1 were separately derived (Table S1) (Lanie *et al.*, 2007, Pozzi *et al.*, 1996). Laboratory strain R800 was further derived from strain R6 (Lefevre *et al.*, 1979). To complicate things further, the genome sequences of different isolates of the same laboratory strain have diverged. For example, R6 has at least 80 additional mutations than its progenitor, D39 (Lanie *et al.*, 2007), whereas Rx1, which contains a defect in mismatch repair, can contain as many as 600 additional mutations compared to R6 (Yanina Tovpeko and Marco Oggioni, personal communications). Reflecting these different genetic backgrounds, *gpsB* is essential in the D39 progenitor strain (Fleurie *et al.*, 2014b, Land *et al.*, 2013), nearly essential in strain Rx1 (Table 1), but not at all essential in R800 or R6 (Table 1) (Fleurie *et al.*, 2014b). Epistasis of Δ*divIVA* mutations to Δ*gpsB* mutations (Fleurie *et al.*, 2014b) is confined to the R800 background and was not observed in the D39, R6, and Rx1 strains (Fig. 1 and S1). Likewise, a requirement for GpsB to localize StkP to septal rings is confined to the R800 strain and was not observed for other *Spn* strains (Fig. 7 and S9). Given that laboratory strains have been mutagenized and selected in culture to optimize specific traits, the chance of characterizing primary cell division mechanisms, rather than bypass mechanisms, is greater in strains derived directly from virulent progenitor strains, such as D39, instead of domesticated laboratory strains containing many additional mutations (Lanie *et al.*, 2007). By starting with bypass mutants, it is difficult to determine the mechanisms that operate in wild-type, virulent *Spn* strains.

Activation of protein phosphorylation by GpsB

Since *gpsB* is essential in D39 derivatives, but not laboratory strains, we isolated bypass suppressors in the D39 Δ*cps* background to better understand the role of GpsB in cell division (Table 2). Three categories of Δ*gpsB* suppressors were found. In this paper, we focus on the mutations that inactivate the *phpP* protein phosphatase (D192A, G229D, and L148S) (Table 2; Fig. S4) or that abolish protein phosphorylation altogether (*sup 2* and *sup3*, Table 2; Fig. 3 and S3). Western analyses confirmed the previous conclusion (Fleurie *et al.*, 2014b) that GpsB depletion in the D39 Δ*cps* strain or Δ*gpsB* mutations in R6 or Rx1 significantly reduced the level of protein phosphorylation by the single StkP protein kinase in *Spn* (Fig. 2). Original or genetically reconstructed D39 Δ*cps* Δ*gpsB* suppressor strains containing *phpP* mutations (Fig. 4), which eliminate protein dephosphorylation (Fig. S4)

(Novakova *et al.*, 2005), restore the level of protein phosphorylation (Fig. 2 and 3). This result is consistent with the idea that GpsB positively activates protein kinase activity, as proposed previously for *Spn* StkP and *Bsu* PrkC (Fleurie *et al.*, 2014b, Pompeo *et al.*, 2015), although it does not rule out the alternative explanation that GpsB negatively regulates PhpP phosphatase activity instead.

Activation of StkP kinase activity by GpsB is implied by several additional findings. In *Bsu*, phosphorylation of GpsB by PrkC seems to play a role in a negative feedback loop (Pompeo *et al.*, 2015). However, phosphorylation of GpsB by StkP was not detected in *Spn* (Fleurie *et al.*, 2014b, Pompeo *et al.*, 2015), and we were unable to detect a GpsB~P species by Phos-tag PAGE (see (Zheng *et al.*, 2016)) in the D39 Δ*cps* parent strain or in the D39 Δ*cps* Δ*phpP*::P_c-*erm* mutant that contains fully phosphorylated DivIVA~P (Fig. 3; data not shown). Previous binding assays of purified proteins indicate a modest interaction between *Spn* GpsB and the cytoplasmic kinase domain of StkP (Fleurie *et al.*, 2014b), and a weak interaction between GpsB and StkP was detected by B2H analyses (Table 4; Fig. S15). To date, we have been unable to clone *Spn* PhpP in the B2H vectors in *Eco*. Notably, GpsB and StkP were detected together in prominent crosslinked complexes from exponentially growing *Spn* cells (Table 4; Fig. 9 and S14). It is not yet possible to tell at which stage of cell division GpsB and StkP are in the same complex, because these cells were not synchronized. In contrast, complexes containing GpsB and PhpP were not detected (Table 4; Fig. 9), and there currently is no evidence that GpsB negatively regulates PhpP phosphatase activity. Protein localization and defects in cell morphology also do not definitively distinguish between GpsB acting as a positive or negative regulator of StkP or PhpP activity, respectively. Results presented here show that GpsB and StkP exhibit different, but overlapping localization patterns at each stage of cell division, and epitope-tagged StkP localization was interfered with by epitope-tagged GpsB (Fig. 6F). Previous results show that GFP-PhpP exhibits diffuse localization over entire cells, with some concentration at septa (Beilharz *et al.*, 2012). This pattern more closely matches that of GpsB than StkP (Fig. 6). Finally, both Δ*stkP* mutants and strains overexpressing PhpP protein phenocopy GpsB depletion (Beilharz *et al.*, 2012, Land *et al.*, 2013, Ulrych *et al.*, 2016). In all three cases, *Spn* cells elongate, enlarge, and fail to close multiple septa (see Fig. 7 and 8). Additional biochemical assays of purified GpsB and its domains with StkP and PhpP are needed to distinguish whether GpsB activates StkP kinase activity, inhibits PhpP phosphatase activity, or both.

Other classes of Δ*gpsB* suppressors

Besides numerous mutations in *phpP*, two other classes of Δ*gpsB* suppressors were identified (Tables 1 and 2). The *sup2* Δ*gpsB* and *sup3* Δ*gpsB* suppressors contained large deletion/duplications in the *spd_1034* region of the chromosome (Fig. S3). Unexpectedly, the *sup2* and *sup3* suppressors lacked phosphorylated proteins (Fig. 3), despite expressing the $StkP^+$ and $PhpP^+$ proteins. The Δ[*spd_1029–spd_1037*] deletion from the Δ*gpsB sup3* suppressed strain (Table 2, line 3; Fig. S3) did not suppress the Δ*gpsB* mutation or alter protein phosphorylation (see *Results*; Fig. S8), and the mechanism of Δ*gpsB* suppression by these complicated genetic rearrangements remains to be determined. Genetically unstable Δ*stkP* mutants that likely accumulated suppressor mutations also could suppress Δ*gpsB*

mutations (Table 1; *Results*). Together, these observations suggest that another, uncharacterized level of regulation of protein phosphorylation, cell division, or both operates in *Spn*. Additional Δ*gpsB* suppressor mutations that did not affect protein phosphorylation or the *spd_1034* region of the chromosome were found (Table 2) and are being characterized.

Regulation of PBP activities by GpsB

Another phenotype lends support to the conclusion that complexes containing GpsB and StkP control PG biosynthesis in *Spn*, even though GpsB is not a substrate of StkP kinase activity (Fig. 10). Migration of bPBP2x TP activity to the centers of division septa does not occur when GpsB is depleted (Fig. 8), suggesting some form of regulation of bPBP2x by GpsB. This regulation may be mediated by an interaction between GpsB and StkP (Fig. 10). Previous work demonstrated that StkP interacts with bPBP2x through their extracellular PASTA and pedestal domains, respectively (Morlot *et al.*, 2013), although bPBP2x, like GpsB, is not phosphorylated by StkP in *Spn* (unpublished results) (Morlot *et al.*, 2013). Consistent with this conclusion, a complex containing StkP and bPBP2x was detected by *in vivo* co-IP, whereas GpsB did not pull down bPBP2x (Fig. 9 and S13). Altogether, these results support the model (Fig. 10) that an interaction between GpsB and StkP activates bPBP2x to close septal rings, thereby accounting for the multiple unconstricted rings observed in strain D39 depleted for GpsB (Fig. 8) (Land *et al.*, 2013) or deleted for StkP (Beilharz *et al.*, 2012).

This study also suggests that GpsB controls the activities of two other PBPs. Previous structural characterization showed that the dimeric amino terminal domain of GpsB contains a distinctive, negatively charged channel that binds to the cytoplasmic, positively charged amino terminus of *Bsu* aPBP1 and *Lmo* aPBPA1 (Claessen *et al.*, 2008, Cleverley *et al.*, 2016, Rismondo *et al.*, 2016). Given that hexameric GpsB is a trimer of these dimers, this arrangement implies that GpsB binds multiple aPBPs, which may coordinate their activities in PG biosynthesis (Cleverley *et al.*, 2016, Rismondo *et al.*, 2016). Genetic analysis demonstrated that suppressed Δ*gpsB* and Δ*pbp1a* mutations are synthetically lethal in *Spn* (Table 3), suggesting that GpsB activates aPBP2a activity. Consistent with this notion, GpsB could be detected in complexes with aPBP2a, but not with aPBP1a (Fig. 9 and S11). In addition, a recently discovered recognition sequence (Rick Lewis, personal communication) is present in the positively charged, cytoplasmic amino domain of aPBP2a. Together these data provide strong support for the conclusion that GpsB binding directly activates aPBP2a activity. However, the exact role of aPBP2a in pneumococcal PG synthesis remains largely unknown (see (Land & Winkler, 2011, Tsui *et al.*, 2016)).

In addition, results from the co-IP experiments suggest GpsB directly or indirectly regulates bPBP2b TP activity, which is required for peripheral PG synthesis (Berg *et al.*, 2013, Land *et al.*, 2013, Straume *et al.*, 2016, Tsui *et al.*, 2016). One of the first studies of GpsB showed a potential interaction between *Bsu* GpsB and MreC by B2H analysis (Claessen *et al.*, 2008). MreC is involved in peripheral PG synthesis in *Spn* (Fenton *et al.*, 2016, Land & Winkler, 2011, Straume *et al.*, 2016, Tsui *et al.*, 2016). A recent paper claims that *mreC* is not essential in the D39 genetic background (Straume *et al.*, 2016). However, the original Δ*mreC*

mutation, which was polar on downstream *mreD* expression, and new Δ*mreC* mutations that maintain the *mreD* ribosome binding site indicate that *mreC* is indeed essential in strain D39 and that Δ*mreC* mutations can be complemented by ectopically expressed *mreC*$^{+}$ (data not shown) (Fenton *et al.*, 2016). Moreover, new Tn-Seq analysis in D39 shows that both *mreC* and *mreD* are essential genes (Fenton *et al.*, 2016). It seems likely that Δ*mreC* mutant that was claimed to be non-essential in D39 (Straume *et al.*, 2016) acquired a *pbp1a* or another suppressor mutation (Fenton *et al.*, 2016, Land *et al.*, 2013, Tsui *et al.*, 2016).

In support of an interaction between GpsB and MreC, *in vivo* co-IP experiments revealed that GpsB or StkP pulls down MreC, indicating the three proteins are in a complex together at some stage of cell division (Fig. 9 and S14). This interaction between GpsB and MreC implicates GpsB in interacting with and regulating the peripheral PG synthesis machine that includes MreC, MreD, bPBP2b, RodA, MltG, aPBP1a, RodZ, and CozE (Fenton *et al.*, 2016, Philippe *et al.*, 2014, Straume *et al.*, 2016, Tsui *et al.*, 2016). In support of this conjecture, GpsB or StkP pulls down essential bPBP2b required for peripheral PG synthesis (Fig. 9 and S13). We anticipate that additional *in vivo* co-IP experiments will reveal complexes containing GpsB and other component proteins of the peripheral PG synthesis machinery listed above.

Model for GpsB function as a mediator of septal and peripheral PG synthesis in *Spn*

Results and conclusions from this paper can be incorporated into a model that accounts for why GpsB depletion in the D39 progenitor strain causes cells to elongate and enlarge and halts contraction of septal rings (Fig. 9) (Land *et al.*, 2013). According to this model, interactions between EzrA and GpsB coordinate GpsB function with the dynamics of the midcell FtsZ-ring, which mediates both septal and peripheral PG synthesis in ovococcus bacteria (Fig. 10) (see (Land *et al.*, 2013, Massidda *et al.*, 2013, Mura *et al.*, 2016, Tsui *et al.*, 2014)). GpsB functions to balance septal and peripheral PG synthesis by direct or indirect interactions with aPBP2a, bPBP2x, and bPBP2b. GpsB likely activates aPBP2a by a direct interaction between the amino-terminal domains of aPBP2a and GpsB (Fig. 10) (Cleverley *et al.*, 2016, Rismondo *et al.*, 2016). Although the exact function of *Spn* aPBP2a is unknown, aPBP2a and aPBP1a have a synthetic-lethal relationship, and aPBP1a has been implicated in peripheral PG synthesis (Fenton *et al.*, 2016, Land & Winkler, 2011, Paik *et al.*, 1999); therefore, aPBP2a may play some role in peripheral PG synthesis, especially in the absence of aPBP1a. On the other hand, aPBP1a and aPBP2a may concurrently play roles in septal PG synthesis as well (Fig. 10B) (see (Land *et al.*, 2013, Tsui *et al.*, 2016)).

A GpsB binding motif is absent in the amino terminus of bPBP2x, so it seems likely that GpsB regulation of bPBP2x migration to the center of division septa (Fig. 8) is mediated indirectly through an interaction between GpsB and StkP (Fig. 9), which in turn, interacts with and positively regulates bPBP2x activity (Morlot *et al.*, 2003) (Fig. 10). Reduced bPBP2x activity would account for the failure of septal rings to constrict when GpsB is depleted in D39 strains (Fig. 8) (Land *et al.*, 2013). Like bPBP2x, bPBP2b lacks a GpsB binding motif. GpsB is in complexes with both MreC and bPBP2b at some stage of the cell cycle (Fig. 9 and S14). Since MreC and bPBP2b both mediate peripheral PG synthesis (Fenton *et al.*, 2016, Land *et al.*, 2013, Land & Winkler, 2011, Straume *et al.*, 2016, Tsui *et*

al., 2016), the pronounced elongation of *Spn* D39 cells upon GpsB depletion could be accounted for if GpsB acts as a negative regulator of bPBP2b TP activity (Fig. 10). By positively regulating septal PG synthesis and negatively regulating peripheral PG synthesis, GpsB would balance the levels of peripheral and septal PG growth at different division stages to maintain normal cell shape and size.

Finally, we do not yet understand the role of phosphorylation in GpsB function. Our data strongly supports the conclusions that GpsB function is required for optimal protein phosphorylation in *Spn*, that depletion of GpsB severely reduces protein phosphorylation, and that non-polar, non-functional *phpP* mutations restore growth and phosphorylation levels to a Δ*gpsB* mutant (see *Results*). However, how does restoration of protein phosphorylation bypass the requirement for GpsB? In the progenitor D39 background, the role of phosphorylation of single proteins has remained inconclusive (see (Massidda *et al.*, 2013)). DivIVA and MapZ(LocZ) are established substrates of the StkP protein kinase; yet, replacing phosphorylated threonines with alanines and other amino acids does not produce phenotypes indicative of loss of DivIVA function and MapZ(LocZ) function in D39 strains and R6 and Rx1 laboratory strains (Holečková *et al.*, 2015, Massidda *et al.*, 2013). Although GpsB and bPBP2x likely interact with StkP, a phosphorylated form of neither protein can be detected *in vivo*, even in *phpP* mutants (see *Results*). Several explanations could account for bypass of the requirement for GpsB by restoration of protein phosphorylation. The growth defect of *gpsB* mutants may involve the simultaneous under-phosphorylation of several proteins, instead of the single proteins whose phosphorylated threonines have been changed so far. In addition, new studies show that there are additional StkP-phosphorylated proteins that can be detected in a Δ*phpP* mutant of laboratory strain Rx1, at least one of which influences cell division (Ulrych *et al.*, 2016). Last, autophosphorylation of StkP may itself regulate interactions between StkP and other proteins. These hypotheses and the model for GpsB mediation of PBP activities will be tested in ongoing and future studies.

EXPERIMENTAL PROCEDURES

Bacterial strains, plasmids, and growth conditions

Bacterial strains and plasmids used in this study are listed in Tables S1–S3. Bacterial strains were derived from IU1945, an unencapsulated derivative of serotype 2 *Spn* strain D39 (Lanie *et al.*, 2007), from an isolate of the R6 unencapsulated laboratory strain (EL59) (Lanie *et al.*, 2007), or from Rx1, a second unencapsulated laboratory strain (Pozzi *et al.*, 1996). D39 and R6 strains were grown on trypticase soy agar II with 5% (vol/vol) defibrinated sheep blood (TSAII-BA) plates at 37°C in an atmosphere of 5% CO_2. Rx1 strains were grown on tryptone soya agar (Oxoid) or columbia agar (Lab Media Servis, SRO) with 5% (vol/vol) defibrinated sheep blood (TSBA and CBA, respectively) plates at 37°C in an atmosphere of 5% CO_2. D39 and R6 strains were grown in Becton-Dickinson brain heart infusion (BHI) broth at 37°C in an atmosphere of 5% CO_2. Rx1 strains were grown in tryptone soya broth (TSB; Oxoid) or BHI at 37°C in an atmosphere of 5% CO_2. When required, chloramphenicol (4.5 μg/mL), erythromycin (0.25-0.3 μg/mL), tetracycline (0.25–2.5 μg/mL), spectinomycin (150 μg/mL) and/or kanamycin (250 μg/mL) were added to culture media.

Antibodies and fluorescent D-amino acid (FDAA)

Antibodies used in 2D-IFM, Western blotting, and co-IP procedures were as follows. Exact concentrations used are specified in individual experimental procedures. Primary antibodies used were monoclonal mouse M2 anti-FLAG (Sigma, F1804), polyclonal rabbit anti-FLAG (Sigma, F7425), polyclonal rabbit anti-HA (Invitrogen, 71–5500), polyclonal rabbit anti-Myc (ThermoFisher Scientific, PA1-981), polyclonal rabbit anti-phosphothreonine (α-pThr) (Cell Signalling, #9381), anti-StkP (Beilharz *et al.*, 2012), anti-PhpP (Beilharz *et al.*, 2012), anti-MreC (Land & Winkler, 2011), anti-FtsZ (Lara *et al.*, 2005), and anti-FtsA (Lara *et al.*, 2005). Secondary antibodies used were polyclonal goat Alexa-Fluor 488 anti-mouse (Life Technologies, A-11029), polyclonal goat Alexa-Fluor 568 anti-rabbit (Life Technologies, A-11011), and ECL anti-rabbit IgG, horseradish peroxidase linked whole antibody (GE healthcare NA93AV). FDAA TADA (tetramethylrhodamine 3-amino-D-alanine) was synthesized as described previously (Kuru *et al.*, 2012, Kuru *et al.*, 2015) and obtained from Michael VanNieuwenhze.

Growth curves and phase-contrast microscopy of strains

For physiological and morphological analyses of strains, cells were inoculated from frozen glycerol stocks into BHI, serial diluted, and incubated for 12–16 hours statically at 37°C in 5% CO_2 overnight. The next day, cultures from $OD_{620} \approx 0.05$ to 0.4 were diluted into fresh BHI to $OD_{620} \approx 0.003$ and placed under the same growth conditions. Growth was monitored turbidimetrically every 45 min to 1 hour with a Genesys 2 spectrophotometer (Thermo Scientific). For microscopic analyses, samples (1–2 μl) were taken at $OD_{620} \approx 0.2$ and examined using a Nikon E-400 epifluorescence phase-contrast microscope with a 100× Nikon Plan Apo oil-immersion objective (numerical aperture, 1.40) connected to a CoolSNAP HQ^2 charged-coupled device (CCD) camera (Photometrics). Images were processed using NIS-Elements AR software (Nikon), and measurements and calculation of cell width, length, volume, and aspect ratio were performed as described before (Land *et al.*, 2013, Tsui *et al.*, 2016).

Construction of single and double mutants

Transformation of D39, R6, and Rx1 to obtain derivative strains (Table S1) was performed with linear DNA amplicons made by fusion PCR as described previously (Fadda *et al.*, 2003, Tsui *et al.*, 2010). Primers used to construct D39 and R6 derivative strains are listed in Table S2. Primers used to construct Rx1 strains are listed in Table S3. Constructed strains were confirmed by PCR and DNA sequencing of the chromosomal region corresponding to the linear amplicon and surrounding regions.

Rx1 mutant strains were constructed as follows. The Rx1 Δ*gpsB phpP*(L148S) mutant was obtained using a two-step PCR method as previously described (Fadda *et al.*, 2003) using the three sets of primers listed in Table S3. PCR amplicons were purified using a QIAquick PCR purification kit (Qiagen), mixed, and re-amplified in a second PCR using the external primers. The resulting Δ*gpsB::cat* construct (2282 bp) was used to transform competent *Spn* Rx1 cells. A DNA fragment of the corresponding regions not containing the resistance marker was used as a negative control for transformation. Transformants were selected after 24 h growth on TSBA plates containing chloramphenicol (4.5 μg/ml). If no growth was

observed, incubation was extended up to 48 h. Eight transformants were verified by PCR for integration of the construct and four of them stored as frozen glycerol stocks for further analysis. One transformant was sequenced in the *phpP-stkP* region and found to contain a *phpP*(L148S) mutation (bp T443C). The Rx1 Δ*gpsB phpP*(L148S) Δ*divIVA* double mutant was generated by transforming the Δ*divIVA::erm* construct (1844 bp), amplified from chromosomal DNA of a Δ*divIVA* mutant (Fadda *et al.*, 2003) using primers LN235/LN236, into Rx1 Δ*gpsB phpP*(L148S) competent cells. Transformants were selected after 24 h growth on CBA plates containing erythromycin (0.2 μg/ml) and verified for growth on CBA plates containing chloramphenicol and erythromycin, before being stored as frozen glycerol stocks. One transformant, verified for the correct insertion of the construct, was used for further analysis. A clean Rx1 Δ*gpsB* mutant was obtained via transformation of a Δ*gpsB*<>*aad9* amplicon into the Rx1 parent strain, using methods described previously (Tsui *et al.*, 2010). This strain was sequenced in the *phpP-stkP* region and determined to have no mutations.

Construction of *phpP*(D192A)

A *phpP*(D192A)-P_c-[*kanrpsL*$^+$] amplicon was constructed by PCR fusion of 5' and 3' fragments from IU7673. Primer sets TT546/BR26 and BR25/TT574 were used to obtain the fragments. *phpP*(D192A) was obtained by PCR from the full-length *phpP*(D192A)-P_c-[*kanrpsL*$^+$] amplicon using primers TT546/TT580. *phpP*(D192A) was then transformed into IU4888 without fucose, resulting in strains IU10180 and IU10191. *phpP*(D192A) amplicon from IU10180 and IU10191 was then obtained by PCR with primers TT546/TT547 for further experiments.

phpP(G229D) and *phpP*(D192A) allele exchange and Δ*gpsB* suppression confirmation

phpP(G229D) amplicon was obtained from IU6442 (D39 Δ*cps* Δ*gpsB*<>*aad9* *phpP*(G229D)) using primers in Table S2. *phpP*(D192A) amplicon was obtained as described above. As outlined in *Results*, two methods were used to confirm that *phpP*(G229D) or *phpP*(D192A) could suppress Δ*gpsB* in reconstructed strains.

In the first method (Fig. 4A), *phpP*(G229D) or *phpP*(D192A) amplicons were transformed into strain IU7673 (D39 Δ*cps rpsL phpP*$^+$-P_c-[*kan-rpsL*$^+$]-*stkP*$^+$). This transformation yielded both wild-type and tiny sized (1/6th of wild-type) colonies. Tiny colonies were stored and sequenced in the *phpP-stkP* region. Four out of the six resulting strains from the *phpP*(G229D) transformation had *phpP*(G229D), with three being *stkP*$^+$ (IU8805, IU10423, and IU10424) and one having a mutation at G10 resulting in a stop codon in *stkP* (IU7685). Two of the resulting strains were wild-type for both *phpP*$^+$ and *stkP*$^+$ and were not analyzed further. Two out of the three strains from the *phpP*(D192A) transformation retained the *phpP*(D192A) mutation and were *stkP*$^+$ (IU11223 and IU11240). One of the strains was wild-type for both *phpP*$^+$ and *stkP*$^+$. The resulting strains (D39 Δ*cps rpsL phpP*(G229D)-*stkP*$^+$ or D39 Δ*cps rpsL phpP*(D192A)-*stkP*$^+$) were then transformed with Δ*gpsB*<>*aad9* from IU4888 or Δ*purR*<>*aad9* amplicon as a control (Land & Winkler, 2011). This transformation resulted in strains that were *phpP*(G229D) Δ*gpsB* (IU11344, IU11346) or *phpP*(D192A) Δ*gpsB* (IU11348). Mutations in stored colonies were confirmed by PCR, and

sequencing confirmed the presence of Δ*gpsB, phpP*(G229D) *stkP*$^+$, or *phpP*(D192A) *stkP*$^+$. This construction was performed twice with similar results.

In the second method (Fig. 4B), merodiploid strain IU4888 (D39 Δ*cps* Δ*gpsB*<>*aad9*// Δ*bgaA*::Δ*cps* Δ*gpsB*//P_{fcsK}-*gpsB*$^+$), which requires fucose to induce GpsB expression (Land *et al.*, 2013), was grown in the presence of 1.0% (wt/vol) fucose. At OD_{620} ≈ 0.03, 50 ng of *phpP*(G229D) or *phpP*(D192A) amplicon were added to 100 μL of IU4888 and 900 μL of transformation mix without fucose (90% BHI, 10% heat-treated horse serum, 0.18% (wt/vol) glucose, and 100 ng/mL CSP-1), and the mixture was incubated at 37°C in 5% CO_2 for 1 h. The transformation mix was plated on TSAII-BA plates without fucose to select for fucose independent transformants. The absence of fucose (absence of GpsB) allowed for selection of *phpP*(G229D or D192A) cross-in events. Resulting strains [IU10129, IU10138, IU10139, IU10156, and IU10157 for *phpP*(G229D) and IU10180, IU10191, IU10349, IU10350, IU10363 for *phpP*(D192A); Table S1] were confirmed for by PCR and sequencing for the presence of the Δ*gpsB* and *phpP*(G229D) *stkP*$^+$ or *phpP*(D192A) *stkP*$^+$ mutations. This reconstruction experiment was repeated 3× with similar results. Strains were then transformed with a Δ*bgaA*::P_c-*erm* amplicon to replace the Δ*bgaA::kan-t1t2*-Δ*cps* Δ*gpsB*// P_{fcsK}-*gpsB*$^+$ mutation, resulting in strains IU11221 and IU11238. These strains were confirmed by PCR and sequencing for the presence of the Δ*gpsB*, Δ*bgaA*::P_c-*erm*, and *phpP*(G229D) *stkP*$^+$ or *phpP*(D192A) *stkP*$^+$ mutations.

FDAA short-pulse labeling for 2D epifluorescence microscopy

At OD_{620} ≈ 0.15-0.2, live cells were subjected to a short pulse of FDAA labeling for 5 min as described before (Boersma *et al.*, 2015). Resulting FDAA labeled live cells were suspended in 10–20 μL ice-cold PBS, and 1–2 μL of the cell suspension was observed using a Nikon E-400 epifluorescence phase-contrast microscope equipped with a mercury lamp, a 100× Nikon Plan Apo oil-immersion objective (numerical aperture, 1.40), and filter block for fluorescence (Alexa 568, EX 532–587, DM 595, and BA 608–683). Images were taken using a CoolSNAP HQ^2 charged-coupled device (CCD) camera (Photometrics) and processed with NIS-Elements AR software (Nikon). For FDAA (TADA) pictures, an Alexa 568 filter was used with an exposure time of 50–100 ms to visualize labeling.

2D IFM

Localization of FLAG-tagged proteins, HA-tagged proteins, and native StkP by IFM was performed on exponentially growing cells as described before (Land *et al.*, 2013, Tsui *et al.*, 2011). For strains containing one or two epitope-tagged proteins, the primary antibody used was anti-FLAG mouse monoclonal M2 antibody (1:100 dilution) and/or anti-HA rabbit polyclonal antibody (1:100), and the secondary antibody was Alexa-Fluor 488 goat anti-mouse (1:100 dilution) and/or Alexa-Flour 568 goat anti-rabbit (1:100 dilution). For 2D IFM of native StkP, the primary antibody used was anti-StkP rabbit polyclonal antibody (1:1000 dilution), and secondary antibody used was Alexa-Fluor 568 goat anti-rabbit (1:100 dilution). Cells were mounted using mounting media SlowFade gold antifade reagent with DAPI (ThermoFisher/Life Technologies, S36936) and observed by epifluorescence microscopy as described previously (Land *et al.*, 2013). Control experiments with strains containing untagged proteins and the same antibody setups indicated that non-specific

labeling was not detected under these conditions (data not shown). Matlab GUI image analyses of 2D IFM images were performed as described previously (Land *et al.*, 2013).

GpsB depletion experiments

GpsB depletion experiments in D39 Δ*cps* Δ*gpsB*//P_{fcsK}-*gpsB*$^{+}$ merodiploid strain IU4888, which requires fucose addition to induce GpsB expression for growth, were performed as described previously (Land *et al.*, 2013). Bacteria were harvested at OD_{620} ≈ 0.1 and ≈ 0.4 from cultures induced by fucose addition and after 1, 2, and 3 h from cultures lacking fucose to deplete GpsB for Western blot and microscopic analyses.

FDAA labeling of cells depleted for GpsB for 3D-SIM

Serially diluted overnight cultures of wild-type parent IU1945 (D39 Δ*cps*) and GpsB depletion strain IU4888 (D39 Δ*cps* Δ*gpsB*//P_{fcsk}-*gpsB*$^{+}$) (grown in fucose) were diluted to OD_{620} ≈ 0.02 in 3 mL cultures of BHI broth lacking or containing 1.0% (wt/vol) fucose. After 1.5 to 2.5 h of incubation, 500 μL of cultures were centrifuged (16,000×*g* for 5 min). Cell pellets were resuspended in 250 μL of BHI broth containing the FDAA, TADA (final concentration = 500 μM), and incubated for 5 min at 37 °C. Washing and fixation of TADA-labeled cells were performed as described previously (Tsui *et al.*, 2014). Slides were imaged on a DeltaVision OMX 3D-SIM super-resolution imaging system at Indiana University Bloomington Light Microscopy Imaging Center (http://www.indiana.edu/~lmic/microscopes/OMX.html) as described previously (Tsui *et al.*, 2014) using an exposure time of 5 ms at 31% transmittance.

Western blotting analysis and immunodetection

For Western blot analyses using anti-phosphothreonine (α-pThr), anti-StkP, and anti-PhpP antibodies, bacteria were grown exponentially in 5 mL BHI broth to OD_{620} ≈ 0.1 to 0.2–0.5. Aliquots of 1.0 to 1.5 mL were centrifuged (5 min, 13,000×*g* at 25 °C), and cell pellets were put on dry ice. Frozen pellets were resuspended in 20 μL SEDS lysis buffer (0.1% deoxycholate (vol/vol), 150 mM NaCl, 0.2% SDS (vol/vol), 15 mM EDTA pH 8.0) for samples with OD_{620} ≈ 0.1–0.2 and 40–80 μL for samples with OD_{620} ≈ 0.4. Samples were incubated at 37°C for 15 min until cells visibly lysed as determined via phase microscopy. The Bio-Rad DC™ protein assay kit I was used to determine total protein concentrations of samples using a standard curve of 0.1 to 3.0 mg/mL of BSA. Absorbance (750 nm) were determined in a 96-well plate reader (Synergy H1 Hybrid Reader, BioTek). Samples were diluted with 2× Laemlli SDS loading buffer (Bio-Rad) and incubated at 95°C for 10 min. 12.5 μg of total protein was loaded per sample onto a 4–15% precast gradient SDS-PAGE gel (Bio-Rad) and subjected to electrophoresis. Proteins were transferred to a nitrocellulose membrane. StkP proteins, PhpP proteins, and threonine-phosphorylated proteins were detected respectively with anti-StkP (1:50,000), anti-PhpP (1:20,000), or α-pThr (1:2000) (Novakova *et al.*, 2010) as primary antibodies, and ECL anti-rabbit IgG horseradish peroxidase linked whole antibody as secondary (1:10,000). Chemiluminescent signals in protein bands were detected with 1–3 min exposures and quantified using an IVIS imaging system as described in previously (Wayne *et al.*, 2010). To determine relative amounts of threonine-phosphorylated proteins and the PhpP and StkP proteins, luminescence values for each band were subtracted by the value of the background (defined as a box enclosing the

same area of the blot with no detectable signal or from a Δ[*phpP-stkP*]). Background-subtracted amounts are expressed relative to amounts in wild-type or bacteria that were not depleted for GpsB. After blotting, membranes were stained with amido black solution to confirm that protein loading was similar between samples.

Co-immunoprecipitation (Co-IP)

Cultures were grown exponentially in 400 mL of BHI to $OD_{620} \approx 0.25–0.40$. Cells were collected by centrifugation (8,000×*g* for 10 min at 4°C). Cell pellets were washed once with 30 mL of 1X PBS (4°C) and resuspended in 19.8 mL 1X PBS (4°C). 200 μL of 10% paraformaldehyde solution (EMS) were added for crosslinking to a final concentration of 0.1% (vol/vol). Mixtures were incubated at 37°C in an air incubator for 1 h. Cross-linking reactions were quenched by the addition of 4 mL 1.0 M glycine followed by incubation at 25°C for 10 min. Cells were collected by centrifugation (16,500×*g* for 5 min at 4°C). Pellets were washed once with 20 mL cold 1X PBS (4°C) and resuspended in 2 mL of cold lysis buffer (50 mM Tris-HCl pH 7.4, 150 mM NaCl, 1 mM EDTA, 1% Triton X100 (v/v)) with 1 tablet of protease inhibitor (ThermoFisher Scientific, 78429) freshly added per 10 mL of lysis buffer. The suspension was transferred into 2 lysing matrix B tubes (MP Biomedicals) with 1 mL in each tube. Tubes were shaken in FastPrep homogenizer 10× (4×, 5 min on ice, 3×, 5 min on ice, and 3×) with 6.0 M/s for 40 s each at 4°C. Cell debris and lysing matrix from tubes were removed by centrifugation at 16,000×*g* for 5 min at 4°C. Protein concentration of each sample was determined by Bio-Rad DC× protein assay (Bio-Rad). 1 mL of lysate with similar amounts of total protein (5–7 mg/mL) was added to tubes with 50 μL of anti-FLAG magnetic beads (Sigma, M8823). The same amount of protein was loaded onto the beads for strains expressing FLAG-tagged proteins and the corresponding control strains lacking FLAG-tagged proteins in each experiment. The tubes were rotated for 2 h at 4°C. The beads were washed 3 times with 1 mL of lysis buffer (4°C) with 10 min incubation at 4°C each time. FLAG-tagged protein was eluted from the beads by incubation with 100 μL of FLAG elution solution (150 ng 3× FLAG peptide/μL) (Sigma, F4799) for 30 min at 4°C. 100 μL of the elution and of the original lysate added to magnetic beads (input) were separately mixed with 100 μL 2× Laemmli sample buffer (Bio-Rad) containing 5% (vol/vol) β-mercaptoethanol (Sigma) and heated at 95°C for 1 h to break the cross-links. 50–70 μg of input protein samples and 20 μL of each elution sample were separated by SDS-PAGE on 4–15% precast protein gels (Bio-Rad) in Tris-glycine buffer. Gels were subjected to Western blotting using rabbit anti-FLAG (1:2000), rabbit anti-HA (1:1000), rabbit anti-Myc (1:2000), anti-MreC (1:10,000), anti-FtsZ (1:10,000), anti-FtsA (1:10,000), anti-StkP (1:50,000), and anti-PhpP (1:20,000) as primary antibody. Secondary antibody used was ECL anti-rabbit IgG, horseradish peroxidase linked whole antibody (1:10,000). Chemiluminescent signal in protein bands was quantitated by using an IVIS imaging system as described in (Barendt *et al.*, 2009). A mean ratio of band intensity >2 between FLAG tagged and non-FLAG tagged samples was considered as a positive interaction for proteins, with no background subtraction. Each experiment was performed twice independently.

Bacterial two-hybrid (B2H) experiments

B2H experiments were performed according to (Karimova *et al.*, 2005) and Euromedex manufacturer's instructions. For plasmid constructions, *Spn* genes were amplified by PCR

from Rx1 chromosomal DNA, using the primers pairs listed in Table S3. PCR fragments were purified, digested with appropriate restriction enzymes (PstI and BamHI for *gpsB, divIVA, ezrA*, and *ftsZ* and BamHI and EcoRI for *stkP* (New England Biolabs)), and subcloned into the corresponding sites of the BACTH vectors pKNT25 and pUT18 to generate the corresponding hybrid proteins fused at the N-terminal ends of the T25 and T18 fragments. Plasmids were transformed into cloning host, *E. coli* DH5α. After double-strand sequence verification, each pair of plasmids were co-transformed into the *E. coli cya*$^{-}$ strain BTH101 and co-transformation mixtures were spotted onto LB agar plates supplemented with ampicillin (100 μg/mL), kanamycin (50 μg/mL) and X-Gal (40 μg/mL), with or without 0.5 mM IPTG, followed by incubation at 30°C for 36–40 h, as previously described (Karimova *et al.*, 2005). Interactions (or the lack of them) were additionally confirmed by spotting co-transformation mixtures onto M63-0.2% (wt/vol) maltose or M63-0.2% (wt/vol) glucose agar minimal media, supplemented with ampicillin and kanamycin (50 μg/mL and 25 μg/mL, respectively) and X-Gal (40 μg/mL) and onto MacConkey agar supplemented with the appropriate concentrations of ampicillin and kanamycin and 1% (wt/vol) maltose, with incubation times up to 96 h. Plasmid pairs pKNT25/pUT18 and pKT25-zip/pUT18C-zip were used as negative and positive controls, respectively.

Illumina sequencing

Strains IU5844, IU6441, and IU6442 containing spontaneous suppressor mutations that allowed growth of a D39 Δ*cps* Δ*gpsB* deletion mutant were isolated as described in *Results* (see Table 2). Overnight cultures still in exponential phase were diluted into 5 ml of BHI broth to an $OD_{620} \approx 0.01$ and grown to an $OD_{620} \approx 0.3$ to 0.4. Cells were collected by centrifugation (10,000×*g* for 10 min at 25 °C). Genomic DNA was purified using a MasterPure Gram-positive DNA purification kit (Epicenter Biotechnologies) according to the manufacturer's protocol. DNA library construction, Illumina MiSeq DNA sequencing, and bioinformatics analyses were performed as described previously (Tsui *et al.*, 2016). Visual inspection of the coverage data revealed gaps in genomic sequences corresponding to the expected Δ*cps* Δ[*cps2A*-c*ps2H*] and Δ*gpsB* deletion mutations and to the Δ[*spd_1026–spd_1037*] and Δ[*spd_1029–spd_1037*] deletions and adjacent chromosomal duplications in strains IU5845 and IU6441, respectively (see Table 2; Fig. S3). The structures of the rearrangements were verified by assembling the genome sequences using newbler (version 2.9). The resulting contig graph was analyzed to determine the organization of the duplications/deletions (see Fig. S3B).

Analysis of the conservation of G229 among bacterial PP2C phosphatases and protein modeling of *Spn* PhpP and StkP

To determine the conservation of G229 among other bacterial PP2C phosphatases, the NCBI BLASTP v2.2.30+ (Basic Local Alignment Search Tool) interface was used to search for homologous protein sequences among Streptococci and less closely related bacterial species (Altschul *et al.*, 1997, Altschul *et al.*, 2005). The NCBI BLASTP interface was used with preset parameters to search the non-redundant protein sequence database and UniProtKB/Swiss-Prot database for proteins with sequences homologous to the *S. pneumoniae* D39 PhpP amino acid sequence (Protein Accession YP_816996Pa) (The UniProt Consortium, 2013) (Altschul *et al.*, 1997, Altschul *et al.*, 2005).

Amino acid sequences from other previously identified bacterial PP2C phosphatases were obtained to determine conservation of amino acids in *Spn* PhpP involved in Δ*gpsB* suppression. The following phosphatase amino acid sequences were aligned with *S. pneumoniae* PhpP (Novakova *et al.*, 2005) using Clustal Omega (Sievers *et al.*, 2011) on default settings: *S. agalactiae* PP2C phosphatase (Rantanen *et al.*, 2007), *L. monocytogenes* Stp (Archambaud *et al.*, 2005), *B. subtilis* PrpC (Obuchowski *et al.*, 2000), *P. aeruginosa* Stp1 (Mukhopadhyay *et al.*, 1999), and *S. mutans* Pppl (Banu *et al.*, 2010). Amino acid sequences were obtained from the NCBI protein sequence database. The Clustal output file was uploaded to the ConSurf server (Ashkenazy *et al.*, 2016) under the Multiple Sequence Alignment (MSA) section, and default parameters were used to perform a conservation alignment for these sequences only.

To determine how G229D and other changed amino acids in *phpP* suppressor mutants might affect PhpP structure, BLASTP was used to search the PDB database for related protein structures (Altschul *et al.*, 1997, Altschul *et al.*, 2005, Berman *et al.*, 2000, Madej *et al.*, 2012, Wang *et al.*, 2007). This search method identified the previously solved structure of the PhpP homolog Stp1 in *S. agalactiae* (PDB ID: 2PK0) (Rantanen *et al.*, 2007) and others listed in Table S4. Structures were then aligned with the Phyre2 generated PhpP threading model (Kelley & Sternberg, 2009) using PyMOL (Schrödinger, LLC). RMSD and Z-scores for each structural alignment were calculated using PyMOL and the DALI server (Schrödinger, LLC, Holm L. and Rosenstrom P) (See Table S4).

Supplementary Material

Refer to Web version on PubMed Central for supplementary material.

Acknowledgments

We thank Yana Tovpeko and Kevin Bruce for helpful discussions, Yana Tovpeko and Marco Oggioni for unpublished genome sequences of derivatives of strain Rx1, Gouzel Karimova for strains and plasmids for B2H assays and discussing results, Mike VanNieuwenhze for a sample of FDAA, and James Ford, Kurt Zimmer, and Doug Rusch for assistance with Illumina DNA sequencing analyses. This work was supported by NIH grant 1RO1GM113172 and NIH grant 1R01GM114315 (to M.E.W.), by Czech Science Foundation Grants P302/12/0256 and P207/12/1568 (to P.B.), by LR7/2007 grant CRP2-401 from the Autonomous Region of Sardinia (RAS) (to O.M.), by predoctoral Quantitative and Chemical Biology (QCB) NIH institutional training grant T32 GM109825 (to B.E.R. and A.J.P.), and by a predoctoral scholarship from the Sardinia Regional Government (European Social Fund 2007–2013) (to A. M.).

REFERENCES

Agarwal S, Agarwal S, Pancholi P, Pancholi V. Strain-specific regulatory role of eukaryote-like serine/threonine phosphatase in pneumococcal adherence. Infect Immun. 2012; 80:1361–1372. [PubMed: 22311926]

Altschul SF, Madden TL, Schaffer AA, Zhang J, Zhang Z, Miller W, Lipman DJ. Gapped BLAST and PSI-BLAST: a new generation of protein database search programs. Nuc Acids Res. 1997; 25:3389–3402.

Altschul SF, Wootton JC, Gertz EM, Agarwala R, Morgulis A, Schaffer AA, Yu YK. Protein database searches using compositionally adjusted substitution matrices. FEBS J. 2005; 272:5101–5109. [PubMed: 16218944]

Archambaud C, Gouin E, Pizarro-Cerda J, Cossart P, Dussurget O. Translation elongation factor EF-Tu is a target for Stp, a serine-threonine phosphatase involved in virulence of *Listeria monocytogenes*. Molec Microbiol. 2005; 56:383–396. [PubMed: 15813732]

Ashkenazy H, Abadi S, Martz E, Chay O, Mayrose I, Pupko T, Ben-Tal N. ConSurf 2016: an improved methodology to estimate and visualize evolutionary conservation in macromolecules. Nuc Acids Res. 2016; 44:W344–W350.

Banu LD, Conrads G, Rehrauer H, Hussain H, Allan E, van der Ploeg JR. The *Streptococcus mutans* serine/threonine kinase, PknB, regulates competence development, bacteriocin production, and cell wall metabolism. Infect Immun. 2010; 78:2209–2220. [PubMed: 20231406]

Barendt SM, Land AD, Sham LT, Ng WL, Tsui HC, Arnold RJ, Winkler ME. Influences of capsule on cell shape and chain formation of wild-type and *pcsB* mutants of serotype 2 *Streptococcus pneumoniae*. J Bacteriol. 2009; 191:3024–3040. [PubMed: 19270090]

Beilharz K, Nováková L, Fadda D, Branny P, Massidda O, Veening JW. Control of cell division in *Streptococcus pneumoniae* by the conserved Ser/Thr protein kinase StkP. Proc Nat Acad Sci USA. 2012; 109:E905–E913. [PubMed: 22431591]

Berg KH, Stamsas GA, Straume D, Havarstein LS. Effects of low PBP2b levels on cell morphology and peptidoglycan composition in *Streptococcus pneumoniae* R6. J Bacteriol. 2013; 195:4342–4354. [PubMed: 23873916]

Berman HM, Westbrook J, Feng Z, Gilliland G, Bhat TN, Weissig H, Shindyalov IN, Bourne PE. The protein data bank. Nuc Acids Res. 2000; 28:235–242.

Boersma MJ, Kuru E, Rittichier JT, VanNieuwenhze MS, Brun YV, Winkler ME. Minimal Peptidoglycan (PG) Turnover in wild-type and PG hydrolase and cell division mutants of *Streptococcus pneumoniae* D39 growing planktonically and in host-relevant biofilms. J Bacteriol. 2015; 197:3472–3485. [PubMed: 26303829]

Busiek KK, Margolin W. Bacterial actin and tubulin homologs in cell growth and division. Curr Biol. 2015; 25:R243–R254. [PubMed: 25784047]

Claessen D, Emmins R, Hamoen LW, Daniel RA, Errington J, Edwards DH. Control of the cell elongation-division cycle by shuttling of PBP1 protein in *Bacillus subtilis*. Molec Microbiol. 2008; 68:1029–1046. [PubMed: 18363795]

Cleverley RM, Barrett JR, Basle A, Bui NK, Hewitt L, Solovyova A, Xu ZQ, Daniel RA, Dixon NE, Harry EJ, Oakley AJ, Vollmer W, Lewis RJ. Structure and function of a spectrin-like regulator of bacterial cytokinesis. Nature Comm. 2014; 5:5421.

Cleverley RM, Rismondo J, Lockhart-Cairns MP, Van Bentum PT, Egan AJ, Vollmer W, Halbedel S, Baldock C, Breukink E, Lewis RJ. Subunit arrangement in GpsB, a regulator of cell wall biosynthesis. Microbial Drug Resis. 2016; 22:446–460.

Echenique J, Kadioglu A, Romao S, Andrew PW, Trombe MC. Protein serine/threonine kinase StkP positively controls virulence and competence in *Streptococcus pneumoniae*. Infect Immun. 2004; 72:2434–2437. [PubMed: 15039376]

Fadda D, Pischedda C, Caldara F, Whalen MB, Anderluzzi D, Domenici E, Massidda O. Characterization of divIVA and other genes located in the chromosomal region downstream of the dcw cluster in *Streptococcus pneumoniae*. J Bacteriol. 2003; 185:6209–6214. [PubMed: 14526035]

Fadda D, Santona A, D'Ulisse V, Ghelardini P, Ennas MG, Whalen MB, Massidda O. *Streptococcus pneumoniae* DivIVA: localization and interactions in a MinCD-free context. J Bacteriol. 2007; 189:1288–1298. [PubMed: 17098892]

Fenton AK, El Mortagi L, Lau DTC, Rudner TG, Bernhardt TG. Control of cell elongation by a novel member of the S. pneumoniae MreCD complex. Nature Microbiol. 2016; 2:16237. [PubMed: 27941863]

Fleurie A, Cluzel C, Guiral S, Freton C, Galisson F, Zanella-Cleon I, Di Guilmi AM, Grangeasse C. Mutational dissection of the S/T-kinase StkP reveals crucial roles in cell division of *Streptococcus pneumoniae*. Molec Microbiol. 2012; 83:746–758. [PubMed: 22211696]

Fleurie A, Lesterlin C, Manuse S, Zhao C, Cluzel C, Lavergne JP, Franz-Wachtel M, Macek B, Combet C, Kuru E, VanNieuwenhze MS, Brun YV, Sherratt D, Grangeasse C. MapZ marks the

division sites and positions FtsZ rings in *Streptococcus pneumoniae*. Nature. 2014a; 516:259–262. [PubMed: 25470041]

Fleurie A, Manuse S, Zhao C, Campo N, Cluzel C, Lavergne JP, Freton C, Combet C, Guiral S, Soufi B, Macek B, Kuru E, VanNieuwenhze MS, Brun YV, Di Guilmi AM, Claverys JP, Galinier A, Grangeasse C. Interplay of the serine/threonine-kinase StkP and the paralogs DivIVA and GpsB in pneumococcal cell elongation and division. PLoS Genet. 2014b; 10:e1004275. [PubMed: 24722178]

Gamba P, Veening JW, Saunders NJ, Hamoen LW, Daniel RA. Two-step assembly dynamics of the *Bacillus subtilis* divisome. J Bacteriol. 2009; 191:4186–4194. [PubMed: 19429628]

Giefing C, Jelencsics KE, Gelbmann D, Senn BM, Nagy E. The pneumococcal eukaryotic-type serine/threonine protein kinase StkP co-localizes with the cell division apparatus and interacts with FtsZ in vitro. Microbiol. 2010; 156:1697–1707.

Grangeasse C. Rewiring the Pneumococcal cell cycle with serine/threonine- and tyrosine-kinases. Trends Microbiol. 2016; 24:713–724. [PubMed: 27130634]

Holečková N, Doubravová L, Massidda O, Molle V, Buriánková K, Benada O, Kofroňová O, Ulrych A, Branny P. LocZ is a new cell division protein involved in proper septum placement in Streptococcus pneumoniae. mBio. 2015; 6:e01700–e01714.

Hoskins J, Matsushima P, Mullen DL, Tang J, Zhao G, Meier TI, Nicas TI, Jaskunas SR. Gene disruption studies of penicillin-binding proteins 1a, 1b, and 2a in *Streptococcus pneumoniae*. J Bacteriol. 1999; 181:6552–6555. [PubMed: 10515951]

Karimova G, Dautin N, Ladant D. Interaction network among *Escherichia coli* membrane proteins involved in cell division as revealed by bacterial two-hybrid analysis. J Bacteriol. 2005; 187:2233–2243. [PubMed: 15774864]

Kaval KG, Halbedel S. Architecturally the same, but playing a different game: the diverse species-specific roles of DivIVA proteins. Virulence. 2012; 3:406–407. [PubMed: 22722244]

Kelley LA, Sternberg MJ. Protein structure prediction on the Web: a case study using the Phyre server. Nature Protocols. 2009; 4:363–371. [PubMed: 19247286]

Kuru E, Hughes HV, Brown PJ, Hall E, Tekkam S, Cava F, de Pedro MA, Brun YV, VanNieuwenhze MS. In Situ probing of newly synthesized peptidoglycan in live bacteria with fluorescent D-amino acids. Angew Chem Int Ed Engl. 2012; 51:12519–12523. [PubMed: 23055266]

Kuru E, Tekkam S, Hall E, Brun YV, Van Nieuwenhze MS. Synthesis of fluorescent D-amino acids and their use for probing peptidoglycan synthesis and bacterial growth in situ. Nature Protocols. 2015; 10:33–52. [PubMed: 25474031]

Land AD, Luo Q, Levin PA. Functional domain analysis of the cell division inhibitor EzrA. PloS One. 2014; 9:e102616. [PubMed: 25068683]

Land AD, Tsui HC, Kocaoglu O, Vella SA, Shaw SL, Keen SK, Sham LT, Carlson EE, Winkler ME. Requirement of essential Pbp2x and GpsB for septal ring closure in *Streptococcus pneumoniae* D39. Molec Microbiol. 2013; 90:939–955. [PubMed: 24118410]

Land AD, Winkler ME. The requirement for pneumococcal MreC and MreD is relieved by inactivation of the gene encoding PBP1a. J Bacteriol. 2011; 193:4166–4179. [PubMed: 21685290]

Lanie JA, Ng WL, Kazmierczak KM, Andrzejewski TM, Davidsen TM, Wayne KJ, Tettelin H, Glass JI, Winkler ME. Genome sequence of Avery's virulent serotype 2 strain D39 of *Streptococcus pneumoniae* and comparison with that of unencapsulated laboratory strain R6. J Bacteriol. 2007; 189:38–51. [PubMed: 17041037]

Lara B, Rico AI, Petruzzelli S, Santona A, Dumas J, Biton J, Vicente M, Mingorance J, Massidda O. Cell division in cocci: localization and properties of the *Streptococcus pneumoniae* FtsA protein. Molec Microbiol. 2005; 55:699–711. [PubMed: 15660997]

Lefevre JC, Claverys JP, Sicard AM. Donor deoxyribonucleic acid length and marker effect in pneumococcal transformation. J Bacteriol. 1979; 138:80–86. [PubMed: 35523]

Madej T, Addess KJ, Fong JH, Geer LY, Geer RC, Lanczycki CJ, Liu C, Lu S, Marchler-Bauer A, Panchenko AR, Chen J, Thiessen PA, Wang Y, Zhang D, Bryant SH. MMDB: 3D structures and macromolecular interactions. Nucl Acids Res. 2012; 40:D461–D464. [PubMed: 22135289]

Massidda O, Anderluzzi D, Friedli L, Feger G. Unconventional organization of the division and cell wall gene cluster of *Streptococcus pneumoniae*. Microbiol. 1998; 144:3069–3078.

Massidda O, Novakova L, Vollmer W. From models to pathogens: how much have we learned about *Streptococcus pneumoniae* cell division? Environ Microbiol. 2013; 15:3133–3157. [PubMed: 23848140]

Morlot C, Bayle L, Jacq M, Fleurie A, Tourcier G, Galisson F, Vernet T, Grangeasse C, Di Guilmi AM. Interaction of penicillin-binding protein 2× and Ser/Thr protein kinase StkP, two key players in *Streptococcus pneumoniae* R6 morphogenesis. Molec Microbiol. 2013; 90:88–102. [PubMed: 23899042]

Morlot C, Zapun A, Dideberg O, Vernet T. Growth and division of *Streptococcus pneumoniae*: localization of the high molecular weight penicillin-binding proteins during the cell cycle. Molec Microbiol. 2003; 50:845–855. [PubMed: 14617146]

Mura A, Fadda D, Perez AJ, Danforth ML, Musu D, Rico AI, Krupka M, Denapaite D, Tsui H-CT, Winkler ME, Branny P, Vicente M, Margolin W, Massidda O. Roles of the essential protein FtsA in cell growth and division in *Streptococcus pneumoniae*. J. Bacteriol. 2016 pii: JB.00608-16.

Mukhopadhyay S, Kapatral V, Xu W, Chakrabarty AM. Characterization of a Hank's type serine/threonine kinase and serine/threonine phosphoprotein phosphatase in *Pseudomonas aeruginosa*. J Bacteriol. 1999; 181:6615–6622. [PubMed: 10542161]

Nováková L, Bezousková S, Pompach P, Spidlová P, Sasková L, Weiser J, Branny P. Identification of multiple substrates of the StkP Ser/Thr protein kinase in *Streptococcus pneumoniae*. J Bacteriol. 2010; 192:3629–3638. [PubMed: 20453092]

Nováková L, Sasková L, Pallová P, Janecek J, Novotná J, Ulrych A, Echenique J, Trombe MC, Branny P. Characterization of a eukaryotic type serine/threonine protein kinase and protein phosphatase of *Streptococcus pneumoniae* and identification of kinase substrates. FEBS J. 2005; 272:1243–1254. [PubMed: 15720398]

Obuchowski M, Madec E, Delattre D, Boel G, Iwanicki A, Foulger D, Seror SJ. Characterization of PrpC from *Bacillus subtilis*, a member of the PPM phosphatase family. J Bacteriol. 2000; 182:5634–5638. [PubMed: 10986276]

Ortiz C, Natale P, Cueto L, Vicente M. The keepers of the ring: regulators of FtsZ assembly. FEMS Microbiol Rev. 2016; 40:57–67. [PubMed: 26377318]

Osaki M, Arcondeguy T, Bastide A, Touriol C, Prats H, Trombe MC. The StkP/PhpP signaling couple in *Streptococcus pneumoniae*: cellular organization and physiological characterization. J Bacteriol. 2009; 191:4943–4950. [PubMed: 19502404]

Paik J, Kern I, Lurz R, Hakenbeck R. Mutational analysis of the *Streptococcus pneumoniae* bimodular class A penicillin-binding proteins. J Bbacteriol. 1999; 181:3852–3856.

Peters K, Schweizer I, Beilharz K, Stahlmann C, Veening JW, Hakenbeck R, Denapaite D. *Streptococcus pneumoniae* PBP2x mid-cell localization requires the C-terminal PASTA domains and is essential for cell shape maintenance. Molec Microbiol. 2014; 92:733–755. [PubMed: 24655324]

Philippe J, Vernet T, Zapun A. The elongation of ovococci. Microbial Drug Resis. 2014; 20:215–221.

Pompeo F, Foulquier E, Serrano B, Grangeasse C, Galinier A. Phosphorylation of the cell division protein GpsB regulates PrkC kinase activity through a negative feedback loop in *Bacillus subtilis*. Molec Microbiol. 2015; 97:139–150. [PubMed: 25845974]

Pozzi G, Masala L, Iannelli F, Manganelli R, Havarstein LS, Piccoli L, Simon D, Morrison DA. Competence for genetic transformation in encapsulated strains of *Streptococcus pneumoniae*: two allelic variants of the peptide pheromone. J Bacteriol. 1996; 178:6087–6090. [PubMed: 8830714]

Rantanen MK, Lehtio L, Rajagopal L, Rubens CE, Goldman A. Structure of *Streptococcus agalactiae* serine/threonine phosphatase. The subdomain conformation is coupled to the binding of a third metal ion. FEBS J. 2007; 274:3128–3137. [PubMed: 17521332]

Rismondo J, Cleverley RM, Lane HV, Grosshennig S, Steglich A, Moller L, Mannala GK, Hain T, Lewis RJ, Halbedel S. Structure of the bacterial cell division determinant GpsB and its interaction with penicillin-binding proteins. Molec Microbiol. 2016; 99:978–998. [PubMed: 26575090]

Sasková L, Nováková L, Basler M, Branny P. Eukaryotic-type serine/threonine protein kinase StkP is a global regulator of gene expression in *Streptococcus pneumoniae*. J Bacteriol. 2007; 189:4168–4179. [PubMed: 17416671]

Shah IM, Laaberki MH, Popham DL, Dworkin J. A eukaryotic-like Ser/Thr kinase signals bacteria to exit dormancy in response to peptidoglycan fragments. Cell. 2008; 135:486–496. [PubMed: 18984160]

Sievers F, Wilm A, Dineen D, Gibson TJ, Karplus K, Li W, Lopez R, McWilliam H, Remmert M, Soding J, Thompson JD, Higgins DG. Fast, scalable generation of high-quality protein multiple sequence alignments using Clustal Omega. Mol Syst Biol. 2011; 7:539. [PubMed: 21988835]

Strahl H, Hamoen LW. Finding the corners in a cell. Curr Opinion Microbiol. 2012; 15:731–736.

Straume D, Stamsas GA, Berg KH, Salehian Z, Havarstein LS. Identification of pneumococcal proteins that are functionally linked to penicillin-binding protein 2b (PBP2b). Molec Microbiol. 2016; 103:99–116. [PubMed: 27684385]

Sung CK, Li H, Claverys JP, Morrison DA. An rpsL cassette, janus, for gene replacement through negative selection in *Streptococcus pneumoniae*. App Environ Microbiol. 2001; 67:5190–5196.

Tavares JR, de Souza RF, Meira GL, Gueiros-Filho FJ. Cytological characterization of YpsB, a novel component of the *Bacillus subtilis* divisome. J Bacteriol. 2008; 190:7096–7107. [PubMed: 18776011]

Tsui HC, Boersma MJ, Vella SA, Kocaoglu O, Kuru E, Peceny JK, Carlson EE, VanNieuwenhze MS, Brun YV, Shaw SL, Winkler ME. Pbp2x localizes separately from Pbp2b and other peptidoglycan synthesis proteins during later stages of cell division of *Streptococcus pneumoniae* D39. Molecular microbiology. 2014; 94:21–40. [PubMed: 25099088]

Tsui HC, Keen SK, Sham LT, Wayne KJ, Winkler ME. Dynamic distribution of the SecA and SecY translocase subunits and septal localization of the HtrA surface chaperone/protease during *Streptococcus pneumoniae* D39 cell division. mBio. 2011; 2:e00202–e00211. [PubMed: 21990615]

Tsui HC, Mukherjee D, Ray VA, Sham LT, Feig AL, Winkler ME. Identification and characterization of noncoding small RNAs in *Streptococcus pneumoniae* serotype 2 strain D39. J Bacteriol. 2010; 192:264–279. [PubMed: 19854910]

Tsui HC, Zheng JJ, Magallon AN, Ryan JD, Yunck R, Rued BE, Bernhardt TG, Winkler ME. Suppression of a deletion mutation in the gene encoding essential PBP2b reveals a new lytic transglycosylase involved in peripheral peptidoglycan synthesis in *Streptococcus pneumoniae* D39. Molec Microbiol. 2016; 100:1039–1065. [PubMed: 26933838]

Ulrych A, Holečková N, Goldová J, Doubravová L, Benada O, Kofroňová O, Halada P, Branny P. Characterization of pneumococcal Ser/Thr protein phosphatase *phpP* and identification of a novel PhpP substrate, putative RNA binding protein Jag. BMC Microbiol. 2016; 16(1):247. [PubMed: 27776484]

Wang Y, Addess KJ, Chen J, Geer LY, He J, He S, Lu S, Madej T, Marchler-Bauer A, Thiessen PA, Zhang N, Bryant SH. MMDB: annotating protein sequences with Entrez's 3D-structure database. Nuc Acids Res. 2007; 35:D298–D300.

Wayne KJ, Sham LT, Tsui HC, Gutu AD, Barendt SM, Keen SK, Winkler ME. Localization and cellular amounts of the WalRKJ (VicRKX) two-component regulatory system proteins in serotype 2 *Streptococcus pneumoniae*. J Bacteriol. 2010; 192:4388–4394. [PubMed: 20622066]

Zheng JJ, Sinha D, Wayne KJ, Winkler ME. Physiological roles of the dual phosphate transporter systems in low and high phosphate conditions and in capsule maintenance of *Streptococcus pneumoniae* D39. Front Cell Infect Microbiol. 2016; 6:63. [PubMed: 27379215]

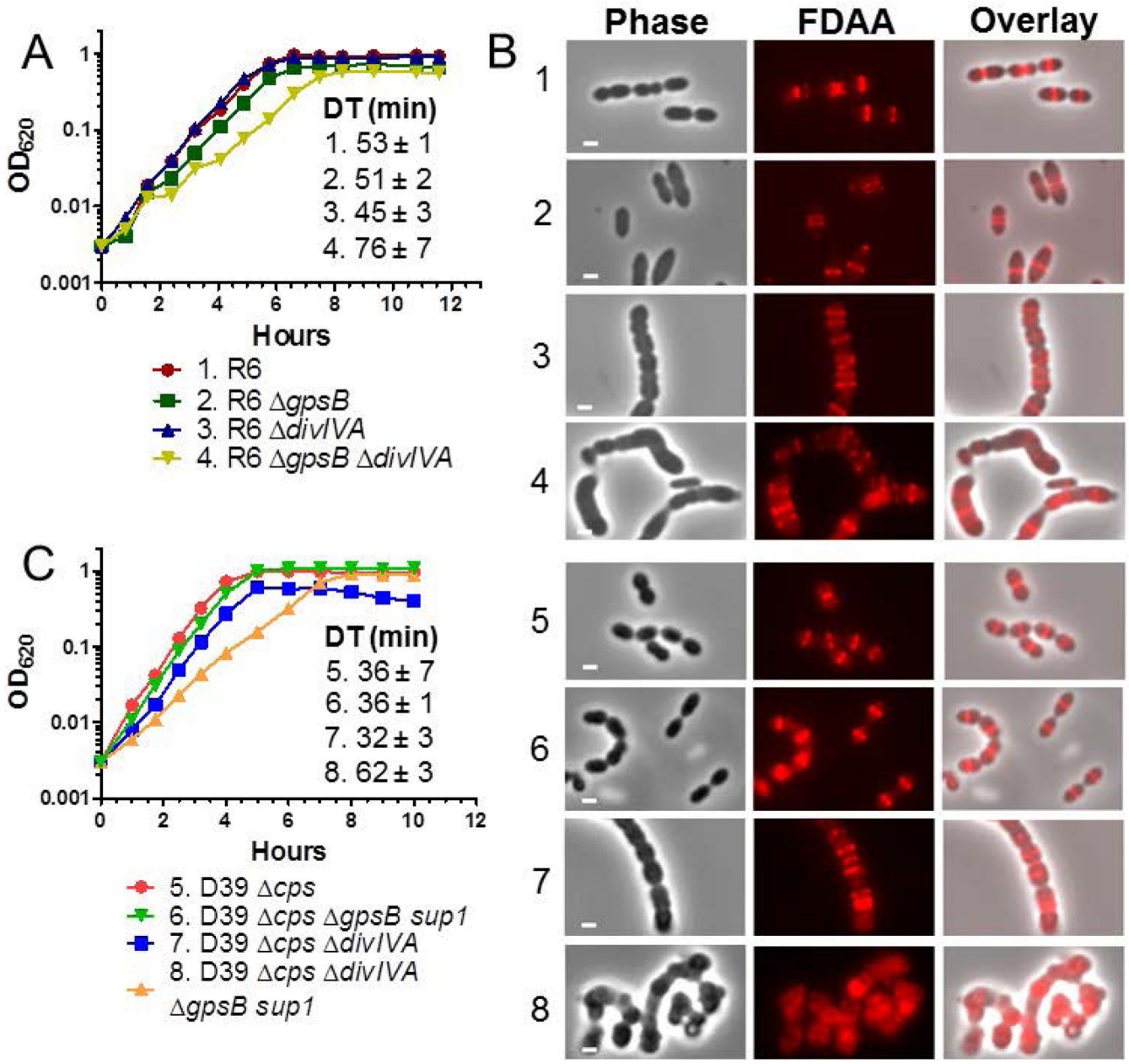

Fig. 1.

Δ*divIVA* mutations are not epistatic to Δ*gpsB* in pneumococcal strains R6 and D39. A) Representative growth curves of R6 strains. Isogenic strains listed as 1–4 are: 1, R6 (EL59); 2, R6 Δ*gpsB* (IU8224); 3, R6 Δ*divIVA* (IU8371); 4, R6 Δ*gpsB* Δ*divIVA* (IU8369). Average doubling times (±SEM) from 2 independent experiments were calculated for $OD_{620} \approx 0.015$ to 0.2 using a nonlinear regression exponential growth curve program (GraphPad Prism). B) Fluorescent D-amino acid (FDAA) staining and microscopy of live cells labeled with FDAA for 5 min were performed as described in *Experimental procedures.* The panels shown from left to right are: phase, FDAA, and a phase/FDAA overlay. Genotypes are indicated according to the numbers in panels A and C. Representative images are shown of ≥95% of the cells (n>50 for R6 strains; n>70 for D39 strains) examined manually of each strain. C)

Representative growth curves of D39 Δ*cps* strains and D39 Δ*cps* Δ*gpsB sup1* strains, which contain a suppressor mutation (*phpP*(G229D)) of Δ*gpsB* as described in the text. Isogenic strains listed as 5–8 are: 5, D39 Δ*cps* (IU1945); 6, D39 Δ*cps* Δ*gpsB phpP*(G229D) (IU6442); 7, D39 Δ*cps* Δ*divIVA* (IU8496); 8, D39 Δ*cps* Δ*gpsB phpP*(G229D) Δ*divIVA* (IU11205). Doubling times were calculated as described above. Independent experiments were performed two to three times with similar results. Scale bar = 1 micron.

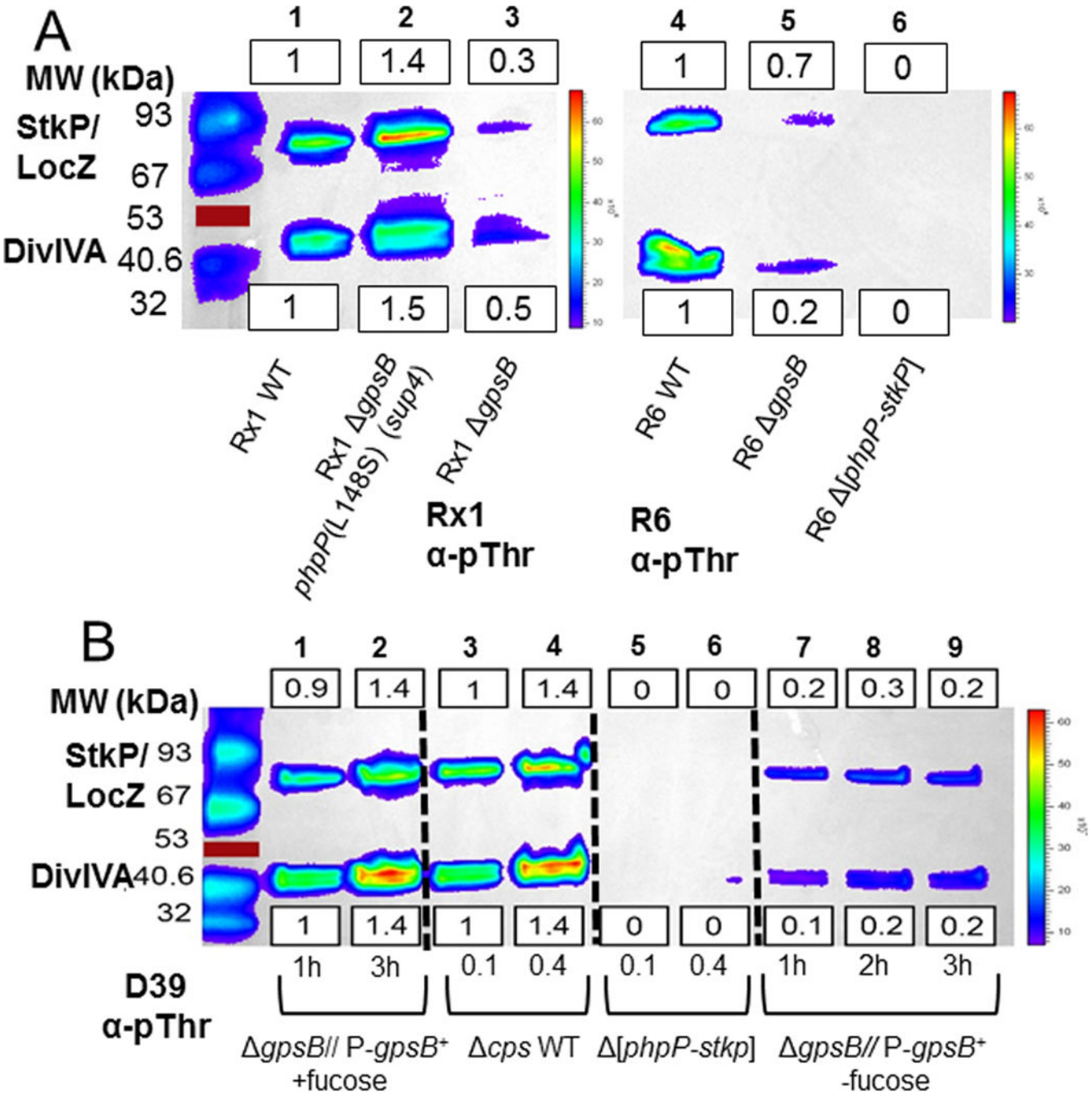

Fig. 2.

GpsB deletion or depletion results in decreased threonine (Thr) phosphorylation of proteins. Proteins phosphorylated on Thr residues were detected by Western blotting with α-pThr antibody, and blots were imaged and quantitated as described in *Experimental procedures*. Equal protein loading was confirmed by amido-black staining of membranes after blotting. Representative blots are shown, with background-subtracted luminescence values relative to the wild-type (wt) strain indicated for the StkP/LocZ and DivIVA bands in boxes above or below the blots, respectively. Relative values of band intensities were calculated as described

in *Experimental procedures*, and mean relative intensities (±SEM) are compiled for all experiments in Table S5 and S6. A) Δ*gpsB* mutants of laboratory strains Rx1 and R6 harvested at $OD_{620} \approx 0.4$. Lane 1, wild-type Rx1 parent (IU9256); lane 2, suppressed Rx1 Δ*gpsB phpP*(L148S) (IU9262); lane 3, Rx1 Δ*gpsB phpP*$^{+}$ *stkP*$^{+}$ (IU11574); lane 4 wild-type R6 parent (EL59); lane 5, R6 Δ*gpsB* (IU8224); and lane 6, R6 Δ[*phpP-stkP*] control (IU8419). The experiment was performed twice independently with similar results. B) GpsB depletion of D39 Δ*cps* strains as described in *Experimental procedures*. Lane 1–2, merodiploid strain Δ*cps* Δ*gpsB*//P_{fcsK}-*gpsB*$^{+}$ (IU4888) grown with fucose for the times indicated; lane 3–4, wild-type parent strain D39 Δ*cps* (IU1945) grown to $OD_{620} \approx 0.1$ or 0.4; lanes 5–6, D39 Δ*cps* Δ[*phpP-stkP*] (E739), and lanes, 7–9, merodiploid strain Δ*cps* Δ*gpsB*//P_{fcsK}-*gpsB*$^{+}$ (IU4888) incubated without fucose for the times indicated. The experiment was performed three times independently with similar results. See text for additional details. Red lines marks a colored 53 kDa standard that did not transfer.

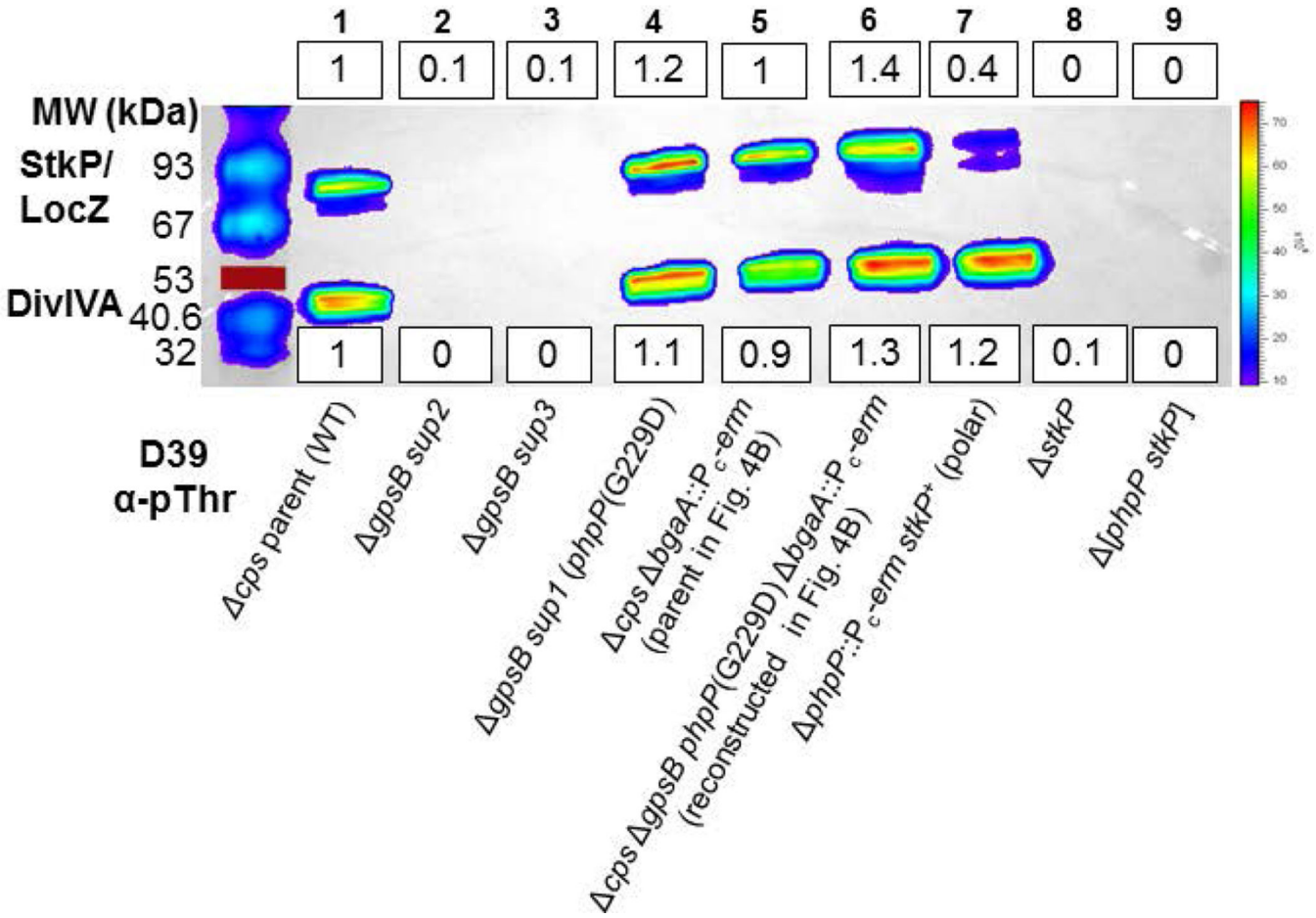

Fig. 3.

phpP(G229D) restores wild-type levels of protein phosphorylation to D39 Δ*cps* Δ*gpsB* mutants in originally isolated and reconstructed suppressor strains. A representative Western blot of phosphorylated proteins was performed and quantitated as described in Figure 2 and *Experimental procedures.* Mean relative values (±SEM) of band intensities are compiled for all experiments in Table S7. Strains were harvested at OD_{620} ≈ 0.4. Lane 1, wild-type parent D39 Δ*cps* (IU1945); lane 2, D39 Δ*cps* Δ*gpsB* Δ[*spd_1026–spd_1037*] Ω[*spd_0889–spd_1026*] (IU5845, *sup2*) (Table 2, line 2); lane 3, D39 Δ*cps* Δ*gpsB* Δ[*spd_1026–spd_1037*] Ω[*spd_0889–spd_1026*] (IU6441, *sup3*); (Table 2, line 3); lane 4, D39 Δ*cps* Δ*gpsB phpP*(G229D) (IU6442, *sup1*) (Table 2, line 1); Lane 5, D39 Δ*cps* Δ*bgaA*::P_c-*erm* (E46) (strain used in reconstruction; Fig. 4B); lane 6, D39 Δ*cps* Δ*bgaA*::P_c-*erm* Δ*gpsB phpP*(G229D) (IU11221) (reconstructed suppressor; Fig. 4B); lane 7, D39 Δ*cps* Δ*phpP*-P_c-*erm* (IU11442) (polar mutant with reduced StkP expression); lane 8, D39 Δ*cps* Δ*stkP* (IU11460) control; and lane 9, D39 Δ*cps* Δ[*phpP-stkP*] (IU11462) control. The experiment was performed twice independently with similar results. The red line marks a colored 53 kDa standard that did not transfer.

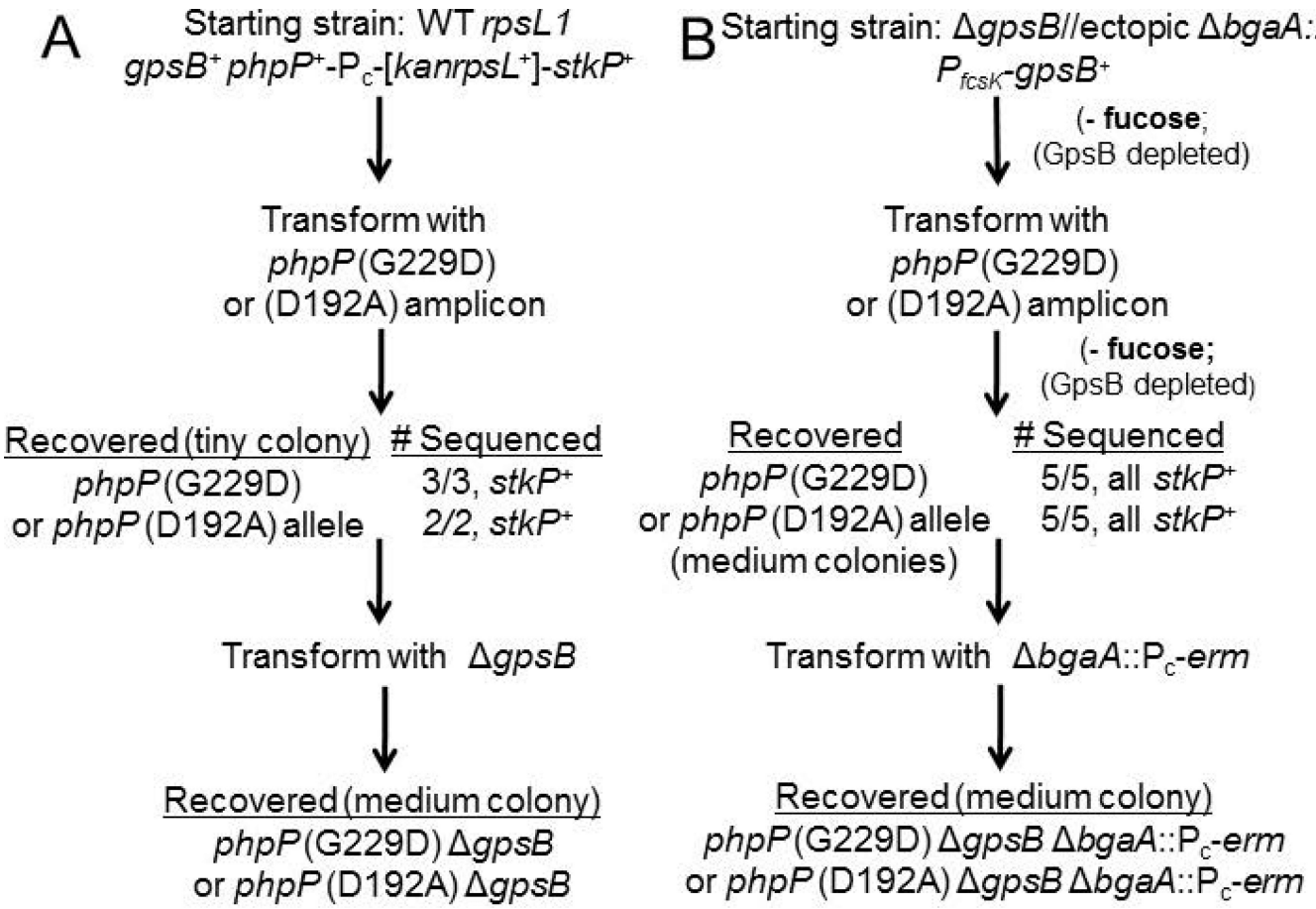

Fig. 4.

Scheme for reconstruction of *phpP*(G229D) or *phpP*(D192A) mutants in D39 Δ*cps rpsL1 gpsB*+ and D39 Δ*cps gpsB*+ genetic backgrounds. See *Experimental procedures* for details. These strains were constructed twice with similar results, and resulting strains are listed in Table S1.

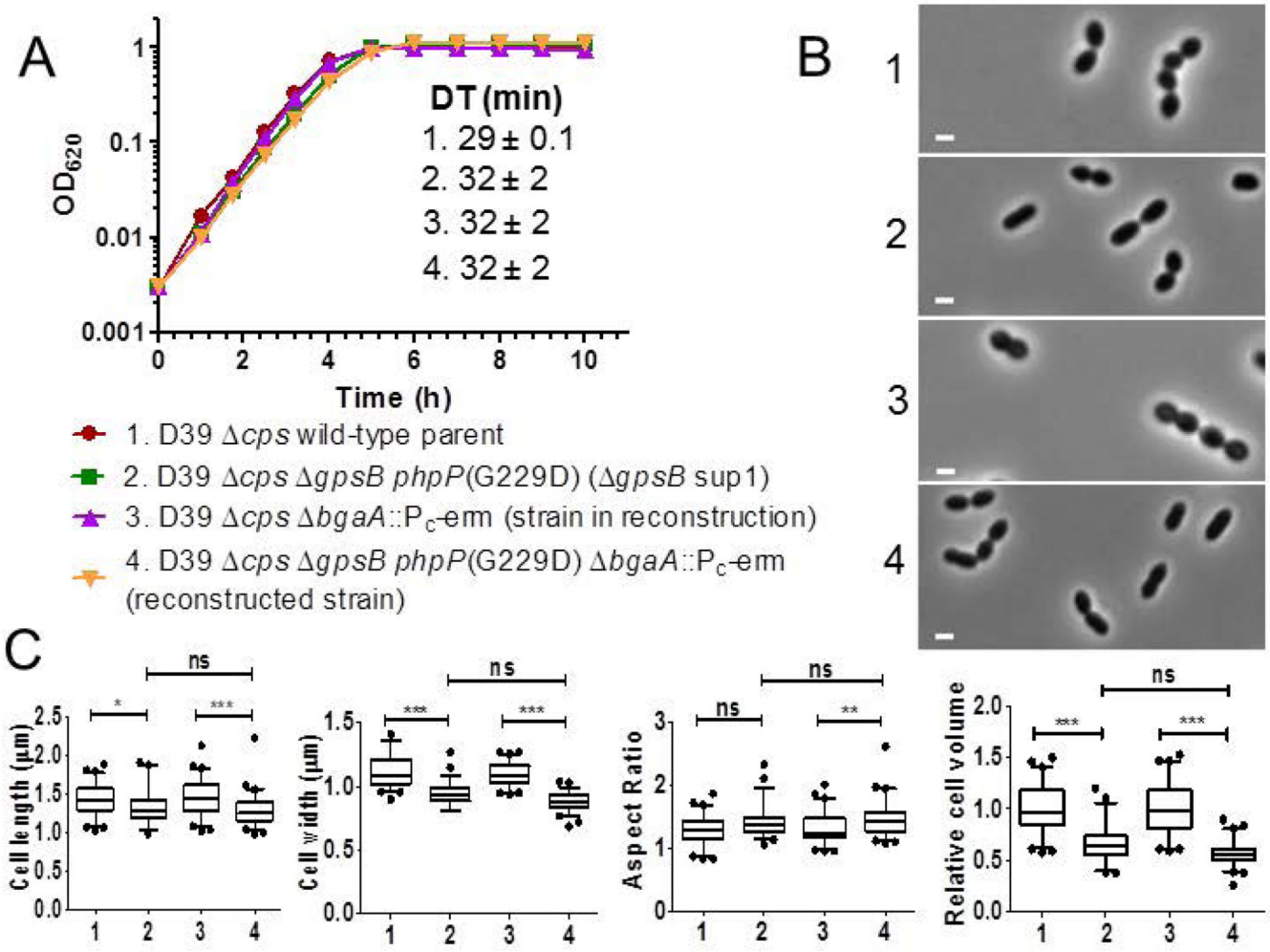

Fig. 5.

D39 Δ*cps* Δ*gpsB phpP*(G229D) suppressor strains grow similarly to wild-type parent strains, but form slightly rounder, smaller-sized cells. A) Representative growth curves of the originally isolated Δ*gpsB sup1* (*phpP*(G229D)) (Table 2, line 1) and reconstructed strain (Fig. 4B). Strain 1, D39 Δ*cps* wild-type parent (IU1945); strain 2, original Δ*gpsB sup1* strain (D39 Δ*cps* Δ*gpsB phpP*(G229D); IU6442, Table 2, line 1); strain 3, E46 used in reconstruction (D39 Δ*cps* Δ*bgaA*::P_c-*erm*; Fig. 4B); strain 4, reconstructed suppressor (D39 Δ*cps* Δ*gpsB phpP*(G229D) Δ*bgaA*::P_c-*erm*; IU11221; Fig. 4B). Doubling times were calculated as described for Figure 1. B) Representative images of live cells at OD_{620} ≈ 0.1–0.2 from growth curves in panel A. C) Length, width, aspect ratio, and cell volume relative to the median value of IU1945 for each strain listed in panel A. Over 50 cells were measured per strain in two experimental replicates. Scale bar = 1 micron.

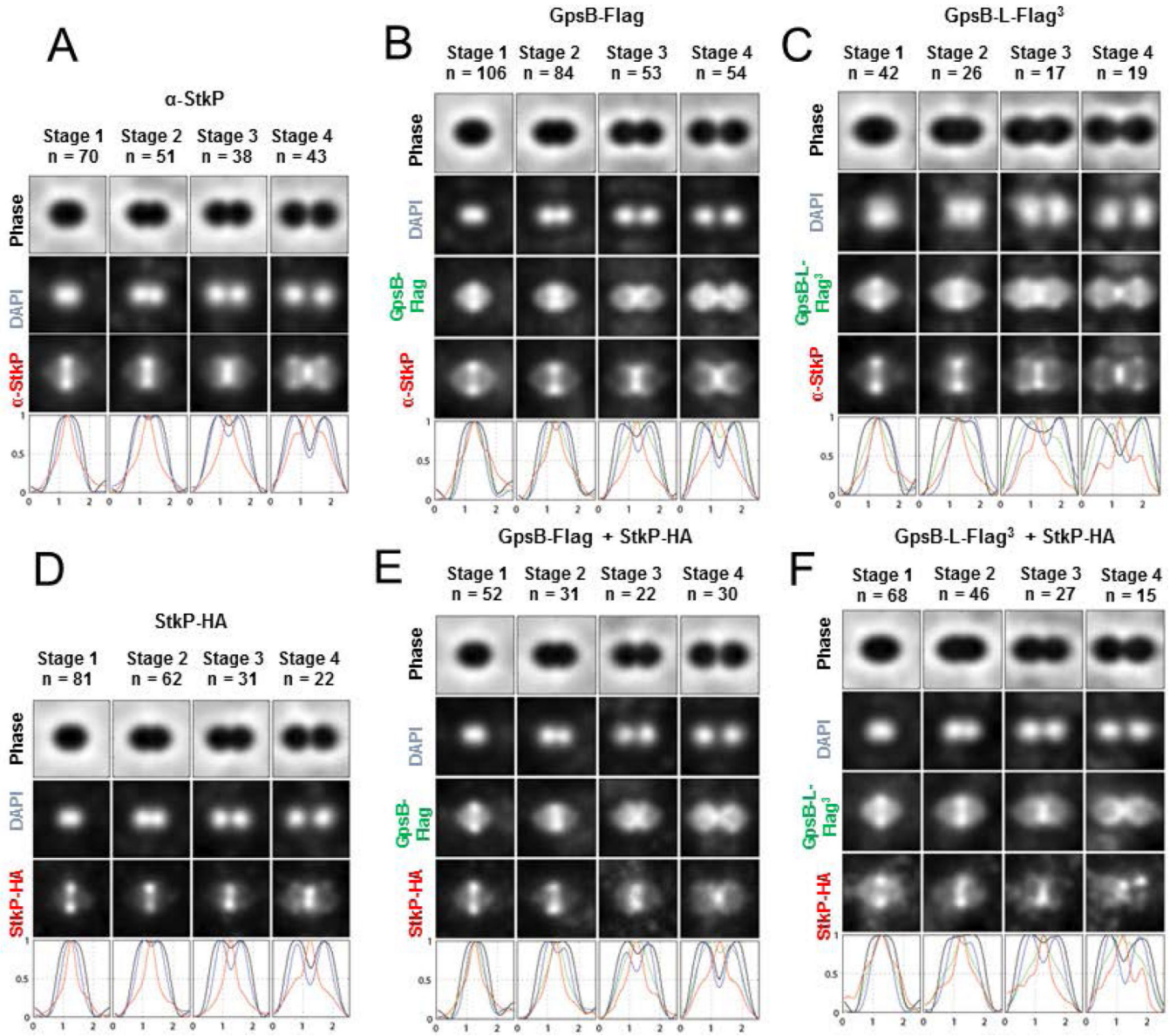

Fig. 6.

GpsB and StkP have different, but overlapping localization patterns at each division stage. Comparison of GpsB and StkP localization by immunofluorescence (IFM) of double- and single-tagged strains and image averaging and quantitation were performed as detailed in *Experimental procedures*. Averaged IFM images of the indicated number of cells at each division stage (n) and fluorescence intensity traces of protein localization are shown for the following strains: A) IU1945 (D39 Δ*cps*) probed with DAPI and anti-StkP antibody; B) IU5838 (D39 Δ*cps gpsB*-FLAG) probed with anti-FLAG and anti-StkP antibodies; C) IU5458 (D39 Δ*cps gpsB*-L-FLAG^3) probed with anti-FLAG and anti-StkP antibodies; D) IU7438 (D39 Δ*cps stkP*-HA) probed with DAPI and anti-HA antibody; E) IU11716 (D39 Δ*cps gpsB*-FLAG *stkP*-HA) probed with anti-FLAG and anti-HA antibody; and F) IU11412 (D39 Δ*cps gpsB*-L-FLAG^3 *stkP*-HA) probed with anti-FLAG and anti-HA antibodies. See text for additional information.

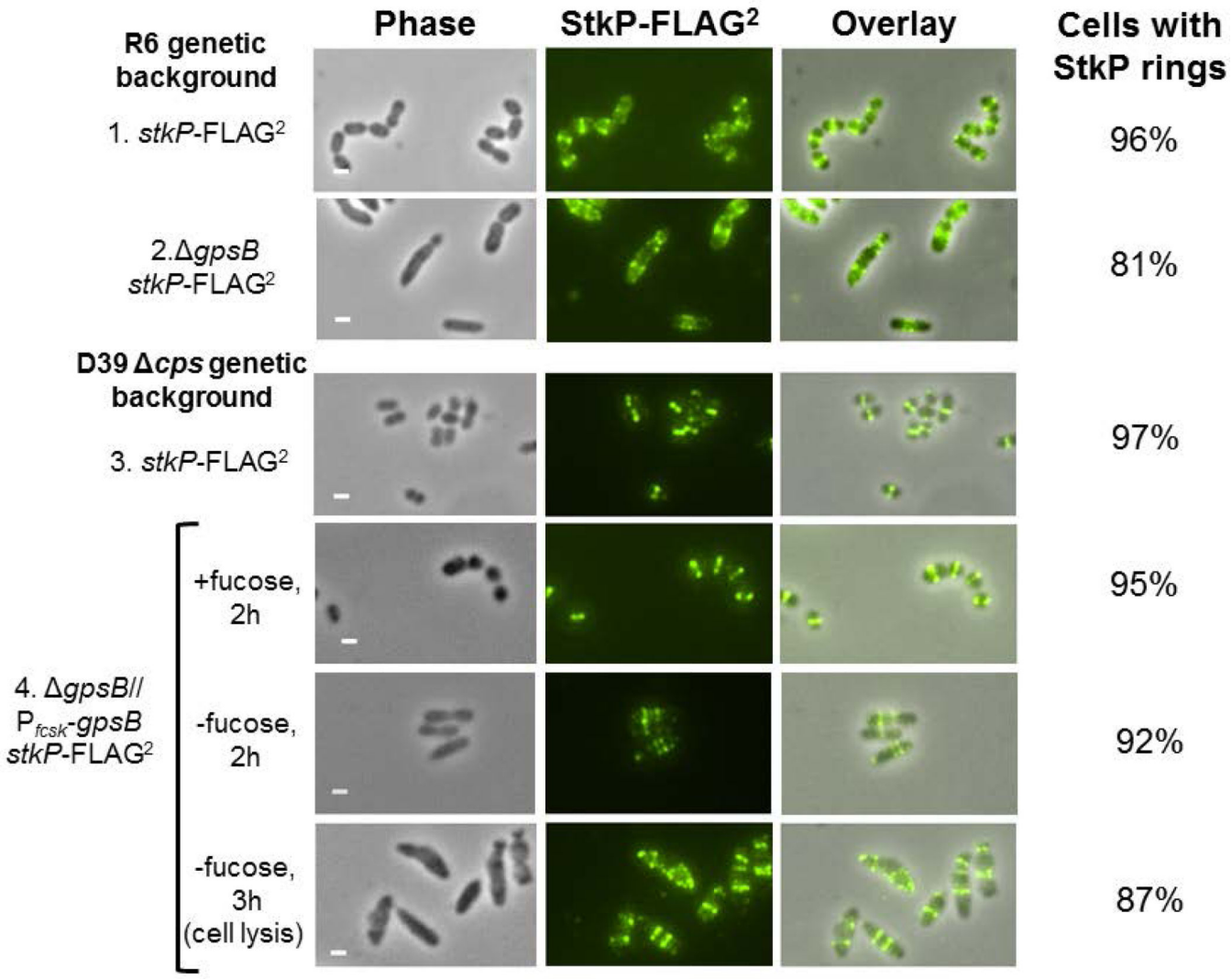

Fig.7.

2D IFM microscopy demonstrates that the absence or depletion of GpsB does not abolish StkP ring formation. 2D IFM was performed as outlined in *Experimental procedures*. Panels shown from left to right are: phase, FITC antibody labeled FLAG-tagged StkP, and phase/FITC overlay. 1) R6 *stkP*-FLAG^2 (IU8819, sampled at $OD_{620} \approx 0.2$); 2) R6 Δ*gpsB stkP*-FLAG^2 (IU8311, sampled at $OD_{620} \approx 0.2$); 3) D39 Δ*cps stkP*-FLAG^2 (IU7434, sampled at $OD_{620} \approx 0.2$); 4) merodiploid strain D39 Δ*cps stkP*-FLAG^2 Δ*cps* Δ*gpsB*//P_{fcsK}-*gpsB*$^+$ (IU8230) grown for 2 h with fucose addition or without fucose for 2 h or 3 h to deplete GpsB, eventually causing cell lysis. Representative images of each strain are shown for each experiment, which were performed three times independently with similar results. Percentages of cells with StkP rings are based on 100 manually examined cells of each strain. Scale bar = 1 micron.

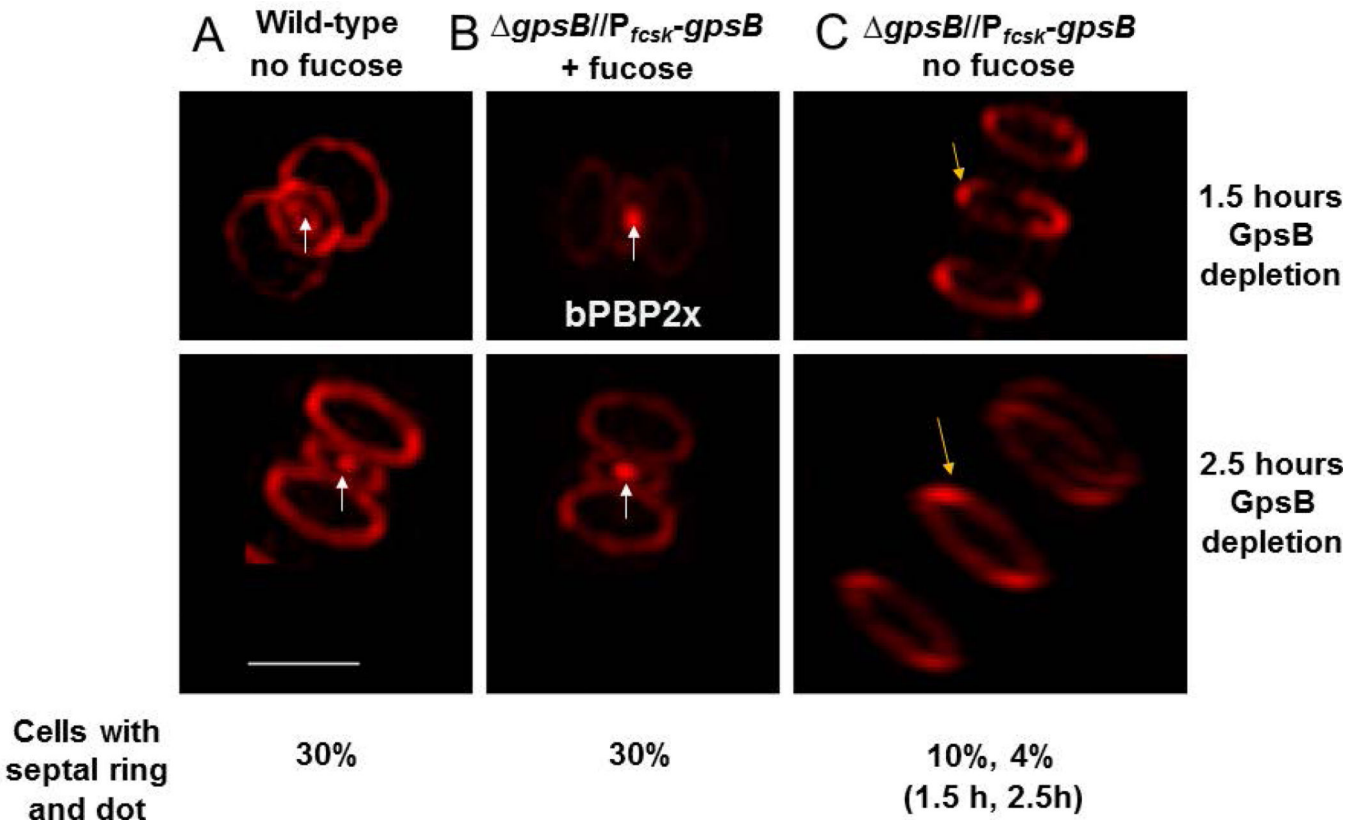

Fig. 8.

GpsB depletion prevents FDAA labeling of septal centers, indicative of bPBP2x migration. Wild-type parent strain IU1945 (D39 Δ*cps*) and *gpsB* merodiploid strain IU4888 (D39 Δ*cps* Δ*gpsB*//P_{fcsK}-*gpsB*$^{+}$) were grown and labeled with FDAA (TADA) as described in *Experimental procedures*. The parent strain and *gpsB* merodiploid strain grown in fucose to induce GpsB expression were growing exponentially at the time of FDAA labeling (A and B), whereas the *gpsB* merodiploid switched to medium lacking fucose was depleted for GpsB for 1.5 h or 2.5 h at the time of FDAA labeling (C). White arrows point to the presence of the central septal spot of FDAA labeling within the septal outer ring in growing cells (A and B). Previous work has shown that this central spot corresponds to bPBP2x TP activity (see text). Yellow arrows point to septal outer rings without central septal spots in elongated cells depleted for GpsB (C). A minimum of 100 cells was observed per condition and strain. Wild-type cells and *gpsB* merodiploid cells grown in fucose had a central septal spot within the septal outer ring ≈ 30% of the time, whereas cells depleted for GpsB for 1.5 h or 2.5 h had a central septal spot within the septal outer ring only 10% or 4% of the time, respectively. The experiment was performed independently twice with similar results. All images are at the same magnification, and scale bar = 1 micron.

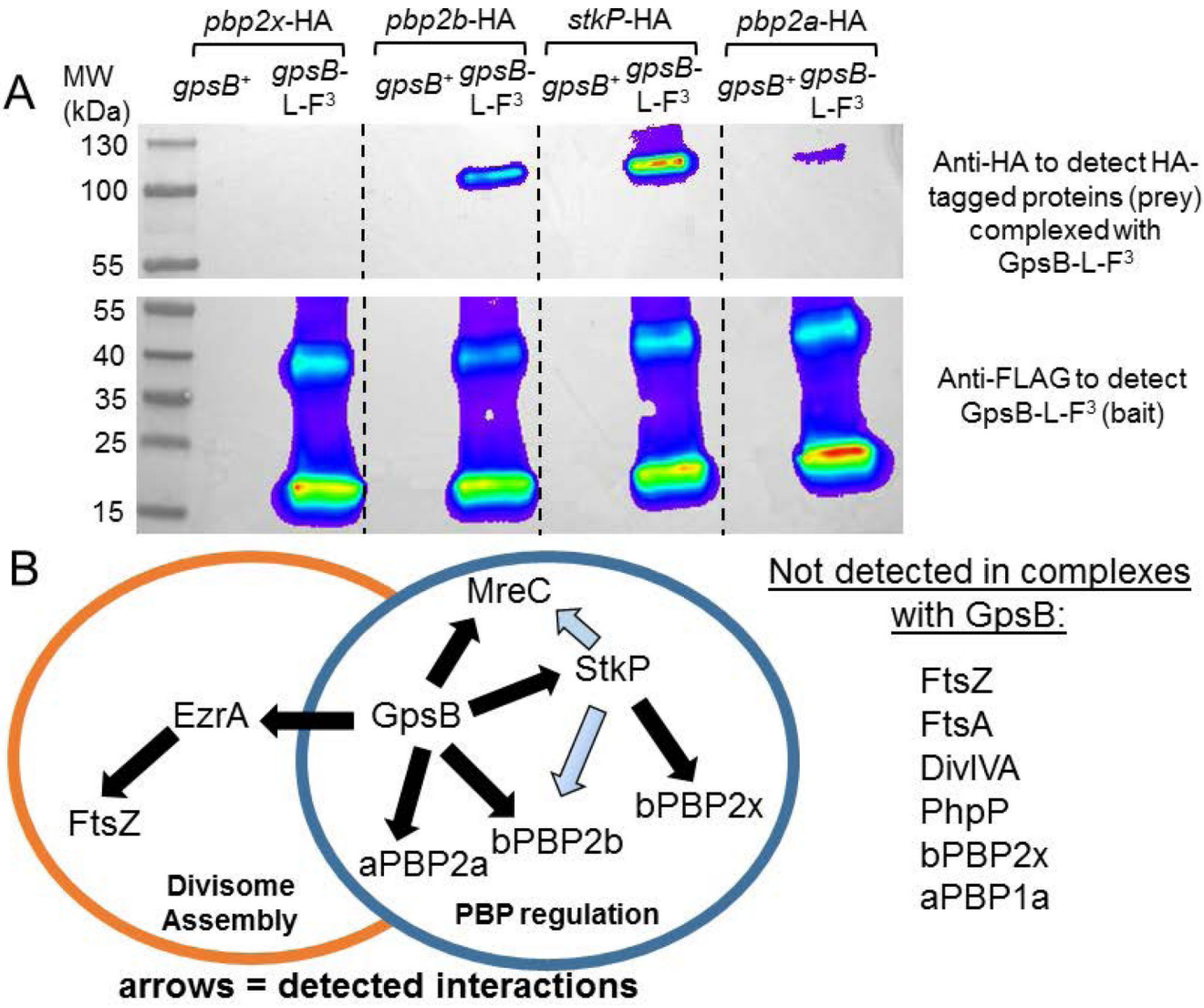

Fig. 9.

A) Pairwise co-IP of GpsB-L-FLAG^3 with bPBP2b-HA, StkP-HA, or aPBP2a-HA^4, but not with bPBP2x-HA. Co-IP experiments were performed as described in *Experimental procedures*. Top blot was probed with anti-HA primary antibody for HA-tagged prey proteins, using GpsB-L-FLAG^3 as bait protein. 57 μg of each lysate sample were loaded on the input gel, while 20 μL of each elution sample was loaded on to the elution gel, after mixing 1:1 with 2× Laemlli sample buffer. Predicted molecular weight (MW) of bPBP2x-HA, bPBP2b-HA, StkP-HA, and aPBP2a-HA^4 are 83.5 kDa, 75.7 kDa, 73.5 kDa, and 85.2 kDa, respectively. Bottom blot was probed with anti-FLAG primary antibody for GpsB-L-FLAG^3 (bait). Two major bands are detected by anti-FLAG primary antibody in strains expressing GpsB-L-FLAG^3. The bottom band correlates to GpsB-L-FLAG^3 monomer (≈ 16.4 kDa), whereas the top band is likely a GpsB-L-FLAG^3 trimer based on MW. Lanes shown on blot are as follows (all strains were constructed in the D39 Δ*cps* background, IU1945): lane 1, *pbp2x*-HA *gpsB*$^+$ (IU6929); lane 2, *gpsB*-L-FLAG^3 *pbp2x*-HA (IU11314); lane 3, *pbp2b*-HA *gpsB*$^+$ (IU6933); lane 4, *gpsB*-L-FLAG^3 *pbp2b*-HA (IU11316); lane 5,

stkP-HA *gpsB*$^{+}$ (IU7438); lane 6, *gpsB*-L-FLAG^{3} *stkP*-HA (IU11412); lane 7, *pbp2a*-HA^{4} *gpsB*$^{+}$ (IU11560); and lane 8 *pbp2a*-HA^{4} *gpsB*-L-FLAG^{3} (IU11516). This experiment was performed twice with similar results. B) Map of interactions found by *in vivo* co-IP that are proposed to coordinate divisome assembly with PBP regulation. GpsB was detected in complexes with EzrA, StkP, aPBP2a, bPBP2b, and/or MreC at stages of the division cycle (above; Fig. S10, S11, and S14). StkP was detected in complexes with bPBP2x, bPBP2b, and MreC (Fig. S13 and S14), although complexes with bPBP2b and MreC could be indirect (blue arrows) via interactions of these proteins with GpsB. EzrA is in complexes with FtsZ and GpsB (Fig. S11 and S12) and other division proteins not shown (Amilcar Perez, in preparation for submission). GpsB did not pull down detectable levels of FtsZ, FtsA, DivIVA, PhpP, bPBP2x, or aPBP1a by this *in vivo* co-IP method (above; Fig. S10–S12 and S14).

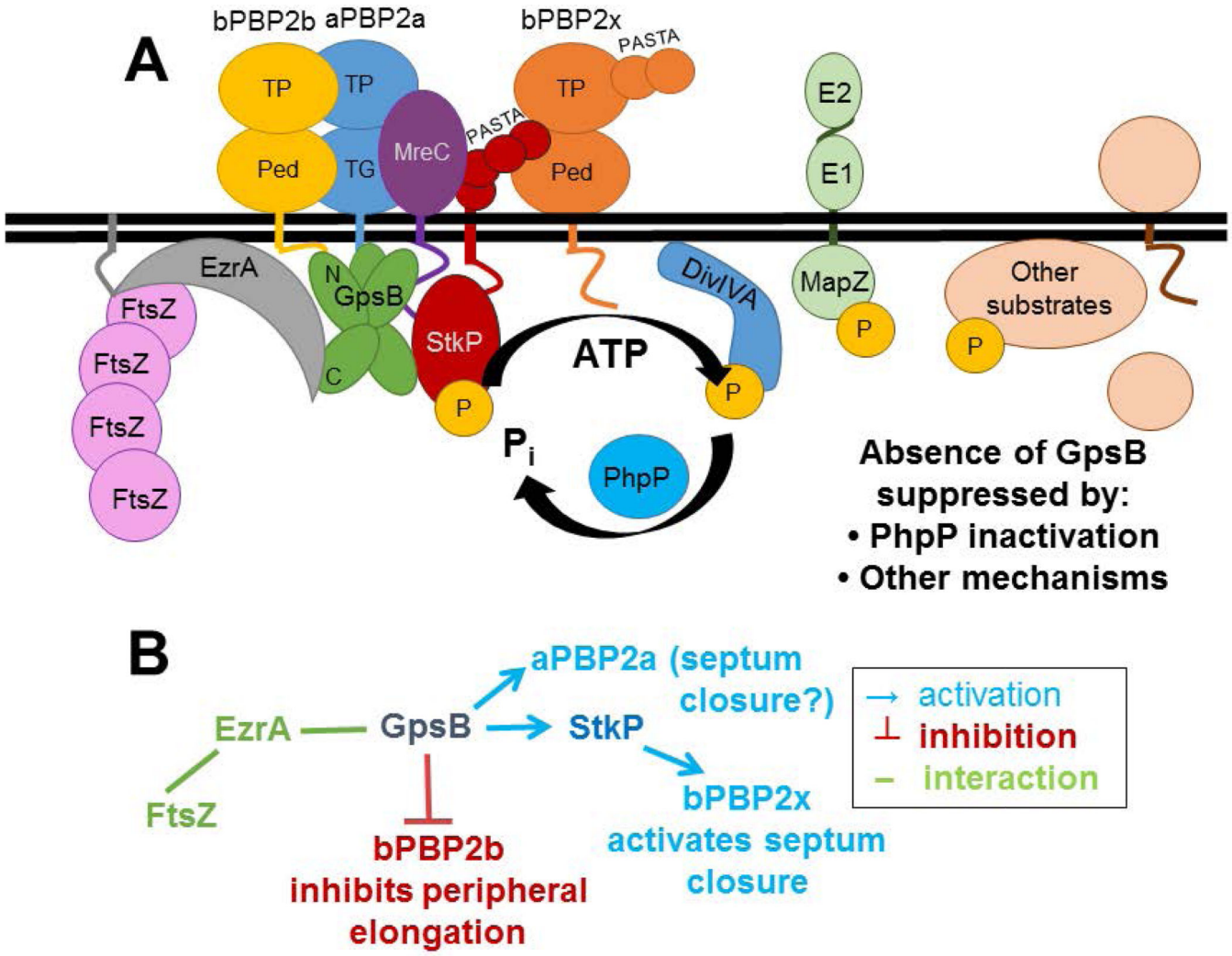

Fig. 10.

Model of GpsB interactions and coordination of septal and peripheral PG synthesis in *Spn* strain D39. A) Complexes containing EzrA, which binds to FtsZ, and GpsB link FtsZ-divisome dynamics (which are not shown) with GpsB regulation of downstream functions. Wild-type levels of GpsB mediate the normal protein phosphorylation cycle by StkP kinase and PhpP phosphatase of numerous division proteins, including DivIVA, MapZ(LocZ), whose extracellular E1 and E2 domains are labeled, and other proteins. Septal and peripheral PG synthesis are coordinated by GpsB complexed with aPBP2a, bPBP2b, MreC, and StkP, which interacts with bPBP2x. bPBP2x and possibly aPBP2a catalyze septal ring closure, whereas bPBP2b and MreC catalyze peripheral PG synthesis. Deletion of *gpsB* is lethal and can be suppressed by non-polar mutations that inactivate the PhpP phosphatase, thereby implicating maintenance of protein phosphorylation levels as an important regulatory function of GpsB; however, the critical phosphorylated protein(s) remain to be determined. B) Genetic scheme of PBP activation by GpsB that can account for the enlarged, elongated cells with unconstricted septa caused by GpsB depletion. According to this scheme, which is based on phenotypes, genetic relationships, microscopy, and interaction maps, GpsB

positively regulates septum closure by activating aPBP2a directly and bPBP2x indirectly, via an interaction between GpsB and StkP, whereas GpsB directly or indirectly inhibits bPBP2b/MreC and peripheral PG elongation. See text for additional details.

TABLE 1

Transformation efficiencies with a Δ*gpsB*<>*aad9* amplicon and colony sizes of recipient and transformant strains[a]

Recipient strain and condition	Genotype of recipient (colony size relative to wild-type (WT) parent strain)	Number of Δ*gpsB*<>*aad9* transformants at 24 h (colony size after streaking; strain)
IU1945 (D39 Δ*cps*) genetic background		
1. IU1945	WT	0[b]
2. IU4846 − fucose	Δ*bgaA*::P_{fcsK}-*gpsB* (WT)	<20 (variable; Land *et. al*, 2013)
3. IU4846 + fucose[c]	Δ*bgaA*::P_{fcsK}-*gpsB* (WT)	>500 (WT; Land *et. al*, 2013)
4. IU11442	Δ*phpP*::P_c-*erm* (small)	20–100 (medium; IU11508)[d]
5. IU7922	Δ*stkP*::P_c-[*kan-rpsL*$^+$] (medium)	20–100 (medium: IU10109)[d]
6. IU11460	Δ*stkP*::P_c-*erm* (medium)	20–100 (medium; IU11546)[d]
7. IU11462	Δ[*phpP-stkP*]::P_c-*erm* (medium)	20–100 (medium; IU11512)[d]
8. K739	Δ[*phpP-stkP*]::P_c-[*kan-rpsL*$^+$] (medium)	20–100 (medium; IU10107)[d]
IU1824 (D39 Δ*cps rpsL1*) genetic background		
9. IU1824	WT	0
10. IU7685	*phpP*(G229D) *stkP*(G10stop) (medium)	≈ 200 (medium; IU7733)
11. IU10423	*phpP*(G229D) (tiny)	≈ 100 (medium; IU11346)
12. IU11223	*phpP*(D192A) (tiny)	>500 (medium; IU11348)
IU1690 (D39 *cps*$^+$) genetic background		
13. IU1690	WT	0[e]
14. IU11183	Δ*phpP*::P_c-*erm* (small)	16–20 (medium; IU11350)
15. IU11456	Δ*stkP*::P_c-*erm* (medium)	≈ 30 (medium; IU11504)
16. IU11458	Δ[*phpP-stkP*]::P_c-*erm* (medium)	≈ 30 (medium; IU11506)
IU1781 (D39 *cps*$^+$ *rpsL1*) genetic background		
17. IU1781	WT	0
18. IU11195	*phpP*(G229D) (tiny)	≈ 30 (small; IU11352)
19. IU11227	*phpP*(D192A) (tiny)	≈ 30 (small; IU11354)
R6 or Rx1 genetic background		
20. R6 (EL59)	WT	>500 (medium; IU8224)
21. Rx1 (IU9256)	WT	≈ 300 (tiny; IU11574)[f]

[a] Recipient strains are described in Table S1. Transformations and visualization of colonies were performed as described in *Experimental procedures*. The numbers of colonies are normalized to 1 mL of transformation mixture. Similar results were obtained for each D39 Δ*cps*, Rx1, or R6 strain from at least two independent transformation experiments in which multiple isolates were examined. Transformation experiments of D39 *cps*$^+$ strains was performed once.

[b] 0 to <10 colonies were visible after 24 h of incubation from >20 independent transformations. Suppressor strain IU5845 appeared ≈ 24 h after transformation, and IU6441 and IU6442 appeared after ≈ 40 h (see text and Table S1). >500 colonies were obtained for transformations of IU1945 with a Δ*purR*<>aad9 control amplicon.

[c] 0.8% (wt/vol) L-fucose was added to all steps in the transformation procedure to induce *gpsB*$^{+}$ expression in merodiploid strain IU4846 (Land *et al.*, 2013).

[d] Numbers of transformants obtained for Δ*phpP* or Δ*stkP* mutants were similar for the Δ*gpsB<>aad9* test and Δ*purR<>aad9* control amplicons within experiments, but varied in independent transformations. This variability is consistent with lower and variable transformation efficiency and recovery of Δ*phpP* or Δ*stkP* mutants reported previously (Echenique *et al.*, 2004, Saskova *et al.*, 2007).

[e] ≈ 80 colonies were obtained for transformation of strain IU1690 with control amplicon Δ*htrA*::P_{C}-*erm*.

[f] Strain IU11574 (Rx1 Δ*gpsB<>aad9*) was isolated from a tiny colony 24 h after transformation of strain Rx1.

Table 2

Analysis of spontaneous Δ*gpsB* suppressor mutations that arose in unencapsulated derivatives of strain D39 and Rx1[a]

Strain number (suppressor designation)	Genetic background	Genotype	Large deletion/ duplication present?[b]	Phosphorylation phenotype[c]	Other mutations present
1. IU6442 (*sup1*)[d]	D39 Δ*cps* Δ*gpsB*	*phpP*(G229D)	No	Normal	None detected; strain reconstructed (see Fig. 4)
2. IU5845 (*sup2*)[e]		Δ[*spd_1026–spd_1037*] Ω[*spd_0889–spd_1026*]	Yes	None	*araD*(ΔC at aa 123/224) *zmpB*(Q456P) *miaA*(N172K)
3. IU6441 (*sup3*)[e]		Δ[*spd_1029–spd_1037*] Ω[*spd_0889–spd_1024*]	Yes	None	None detected
4. IU9262 (*sup4*)[f]	Rx1 Δ*gpsB*	*phpP*(L148S)	No	Normal	*stkP*(I102T) Δ[*spd_1037–spd_1038*]
5. Additional classes of Δ*gpsB* suppressors[g]					

[a] Transformations were performed as described in *Experimental procedures*. Control transformations with a Δ*purR*<>*aad9* amplicons gave >500 colonies in 24 h, whereas Δ*gpsB*<>*aad9* transformations gave <10 colonies in 48 h (see Table 1, line 1). Mutations in the *sup1–3* suppressors were located by whole-genome sequencing (see *Experimental procedures*) and are listed in columns 3 and 6. IU6442, IU5845, and IU6441 grew with similar doubling times (≈ 30 min) as the parent strain in BHI broth, but the growth yields of IU5845 and IU6441 were about 25% lower than those of IU6442 and the parent (Fig. 5A; data not shown).

[b] Chromosomal deletions/duplications Δ[*spd_1026–spd_1037*] (13 genes)/Ω[*spd_0889–spd_1026*] (134 genes) and Δ[*spd_1029–spd_1037*]/Ω[*spd_0889–spd_1024*] are depicted in Figure S3A and 3B.

[c] Detection of proteins phosphorylated at Thr residues was performed by Western blotting using α-pThr antibody as described in *Experimental procedures*. See *Results* and Fig. 3 for details.

[d] Δ*gpsB* suppressor mutants containing *phpP*(G117D) (IU6444), *phpP*(T163P) (IU7736), or *phpP*(R125P) (IU11955) mutations were independently isolated and identified by conventional DNA sequencing of *phpP-stkP*, but were not further characterized in this study. These mutants contained wild-type $stkP^+$ and lacked deletion of the *spd_1034* region, as determined by PCR (Fig. S3).

[e] Deletion in the *spd_1034* region was detected by PCR in 15 additional, independently isolated Δ*gpsB* suppressor mutants that were not characterized further in this study.

[f] *sup4*(*phpP*(L148S)) arose spontaneously in Rx1, which also contained the *stkP*(I102T) and Δ[*spd_1037–spd_1038*] mutations, which were confirmed by conventional DNA sequencing and PCR, respectively.

[g] >5 independent, spontaneous Δ*gpsB* suppressors were isolated that are $phpP^+$ $stkP^+$ and lack deletion in the *spd_1034* region of the chromosome. These suppressors were not further characterized in this study.

Table 3

Synthetic lethality between Δ*pbp1a* and Δ*gpsB* mutations in suppressed strains[a]

Recipient strain	Genotype	Number of colonies at 20 h after transformation with Δ*pbp* amplicons[b]		
		Δ*pbp1a*	**Δ*pbp1b***	**Δ*pbp2a***
EL59	R6	>500	>500	>500
IU8224	R6 Δ*gpsB*	0	>500	>500
IU1945	D39 Δ*cps*	>500	>300	>300
IU6442[c]	D39 Δ*cps* Δ*gpsB* *phpP*(G229D)	0	>300	>300
IU9256	Rx1	>500	>500	>500
IU11574	Rx1 Δ*gpsB*	0	>500	>500
IU9262	Rx1 Δ*gpsB* *phpP*(L148S)	0	>500	>500

[a] Recipient strains were constructed as described in Table S1. Transformations and visualization of colonies from 100 μL or 1 mL of transformation mixture were performed as described in *Experimental procedures*. Zeros (0) indicate no visible colonies after 40 h of incubation. The same results were obtained for each strain from two independent transformation experiments.

[b] Δ*pbp1a*::P_C-e*rm*, Δ*pbp1b*::P_C-e*rm*, and Δ*pbp2a*::P_C-e*rm* amplicons with ≈ 1 kb flanking sequences were obtained from strains E177, E193, and E180 respectively (Table S1). Numbers of colonies indicated were obtained from 1 mL of transformation mixture.

[c] Control transformations of a Δ*gpsB*<>*aad9* amplicon into strains IU1824 (D39 Δ*cps rpsL1*), IU6741 (IU1824 Δ*pbp1a*), IU1945 (D39 Δ*cps*), E180 (IU1945 Δ*pbp2a*::P_C-e*rm*), or E193 (IU1945 Δ*pbp1b*::P_C-e*rm*) resulted in 0 colonies in 20 h, indicating that D39 Δ*cps* Δ*gpsB* Δ*pbp2a* or Δ*gpsB* Δ*pbp1b* strains are only viable when they contain the *phpP*(G229D) suppressor mutation.

Table 4

Complexes containing GpsB and StkP in non-synchronized exponentially growing cells of unencapsulated derivatives of *Spn* D39[a]

	GpsB-L-FLAG^3 as bait in co-IP experiments			
	Prey proteins tested	Primary antibodies in Western blot	Ratio of prey protein band: GpsB-L-FLAG^3 bait to GpsB$^+$ control	Complex detected[b]
	bPBP2b-HA	Anti-HA	18.3 ± 3.1 (n=2)	+
	aPBP2a-HA[4]		4.0 ± 1.2 (n=2)	+
	EzrA-HA		5.4 ± 1.2 (n=2)	+ (+B2H)
[	StkP-HA		22.6 ± 2.4 (n=2)	+ (+B2H)
[	StkP	Anti-StkP	25.7 ±2.4 (n=2)	+ (+B2H)
	MreC	Anti-MreC	6.2 ± 0.4 (n=2)	+
	aPBP1a-HA	Anti-HA	1.9 ±0.7 (n=2)	±
	bPBP2x-HA		1.4 ± 0.0 (n=2)	−
[	HA-FtsA		1.0 ± 0.0 (n=2)	−
[	FtsA	Anti-FtsA	1.2 ± 0.2 (n=2)	−
	DivIVA-Myc	Anti-Myc	1.8 ± 0.3 (n=2)	± (+B2H)
[	FtsZ-Myc		1.3 ± 0.4 (n=3)	− (−B2H)
[	FtsZ	Anti-FtsZ	1.3 ± 0.1 (n=2)	− (−B2H)
	PhpP	Anti-PhpP	0.8 ± 0.0 (n=2)	−
	StkP-FLAG^2 as bait in co-IP experiments			
	Prey proteins tested	Primary antibodies in Western blot	Ratio of prey protein band: StkP-FLAG^2 bait to StkP$^+$ control	Complex Detected
	bPBP2x-HA	Anti-HA	3.4 ± 0.3 (n=2)	+
	bPBP2b-HA		8.1 ± 0.3 (n=2)	+
	MreC	Anti-MreC	8.5 ± 0.1 (n=2)	+
	FtsZ	Anti-FtsZ	1.4 ± 0.4 (n=2)	−
	FtsA	Anti-FtsA	1.6 ± 0.1 (n=2)	−
	PhpP	Anti-PhpP	0.7 ± 0.2 (n=2)	−
	EzrA-L-FLAG^3 as bait in co-IP experiments			
	Prey proteins	Primary antibody in Western blot	Ratio of prey protein band: EzrA-L-FLAG^3 bait to EzrA$^+$ control	Complex Detected
	FtsZ-Myc	Anti-Myc	15.01 ± 10.2 (n=2)	+ (+B2H)

[a]Complexes were detected by pairwise co-IP of the indicated bait and prey proteins from bacterial cells that were crosslinked with paraformaldehyde before lysis as described in *Experimental procedures*. Detection of prey bands by Western blotting (Fig. 9 and S10–S14) is expressed by the mean ratio (±SEM) of luminescence intensity of the prey band recovered from the co-IP to the bait protein compared to the

background area from the control mock co-IP from two or more independent experiments. Brackets indicate testing two different versions of the prey proteins.

[b]+, prey band readily detected; −, prey band not detected; ±, prey band was not visible on blots, or if present, is at the limit of detection by this method; (+B2H), putative direct interaction detected in B2H experiments; (−B2H), direct interaction not detected conclusively in B2H experiment (Fig. S15 and data not shown). B2H assays were performed as described in *Experimental procedures.*